

09,04

## Evolution of the spectral and structural characteristics of borates formed during the interaction of lanthanum and scandium oxides with a potassium tetraborate melt

© S.Z. Shmurak, V.V. Kedrov, A.P. Kiselev, T.N. Fursova<sup>¶</sup>, I.I. Zver'kovaOsipyan Institute of Solid State Physics RAS,  
Chernogolovka, Russia<sup>¶</sup> E-mail: fursova@issp.ac.ru, zverkova@issp.ac.ru

Received March 15, 2023

Revised March 15, 2023

Accepted March 16, 2023

The structure, morphology, IR spectra, as well as luminescence spectra and luminescence excitation spectra of europium-doped borates formed during the interaction of lanthanum and scandium oxides with a potassium tetraborate melt at 970°C with the general formula  $\text{La}_{0.99-x}\text{Sc}_x\text{Eu}_{0.01}\text{BO}_3$  were studied. It is shown that with an increase in the  $\text{Sc}^{3+}$  concentration, three compounds are successively formed:  $\text{LaBO}_3$ ,  $\text{LaSc}_3(\text{BO}_3)_4$ , and  $\text{ScBO}_3$ . At  $0 \leq x \leq 0.26$ , the samples are single-phase and have the structure of  $\text{LaBO}_3$  aragonite. Within the range of  $0.26 < x < 0.75$ , the samples are two-phase and contain the structures of  $\text{LaBO}_3$  aragonite and  $\text{LaSc}_3(\text{BO}_3)_4$  huntite. At  $0.75 \leq x \leq 0.85$ ,  $\text{LaSc}_3(\text{BO}_3)_4$  is observed. Within the range of  $0.85 < x \leq 0.97$ , the samples are two-phase and consist of  $\text{LaSc}_3(\text{BO}_3)_4$  huntite and  $\text{ScBO}_3$  calcite. At  $0.97 < x \leq 0.99$ , the  $\text{ScBO}_3$  samples have a calcite structure. Correspondence between the structure and spectral characteristics of these compounds was established.

**Keywords:** phosphors for LEDs, rare earth orthoborates, X-ray diffraction analysis, IR spectroscopy, luminescence spectra.

DOI: 10.21883/PSS.2023.05.56052.35

### 1. Introduction

Recently, much attention is paid to the investigation of rare earth borates  $\text{ReBO}_3$  ( $\text{Re} = \text{Lu}, \text{Eu}, \text{Tb}, \text{Gd}, \text{La}$ ) and  $\text{ReMe}_3(\text{BO}_3)_4$  ( $\text{Re} = \text{La}, \text{Eu}, \text{Sm}$ ) ( $\text{Me} = \text{Al}, \text{Sc}$ ), since they may be used as high-performance color display phosphors, X-ray phosphors, LED light sources, non-linear crystals [1–7]. To enable these compounds to be used in practice, directional change of their spectral response is essential. Change in structural state of polymorphous phosphors is known to be one of the most efficient methods of their directional emission spectrum change, since each structural modification of borates containing optically active sites has its own unique luminescence spectrum (LS) [8–12]. Luminescence spectra of various structural modifications of borates  $\text{Lu}_{1-x}\text{Re}_x\text{BO}_3:\text{Eu}$  ( $\text{Re} = \text{Gd}, \text{Tb}, \text{Eu}, \text{Y}$ ) and  $\text{Lu}_{1-x}\text{In}_x\text{BO}_3:\text{Eu}$  are studied in [10–15]. These compounds contain  $\text{LuBO}_3$ ,  $\text{ReBO}_3$  and  $\text{InBO}_3$ . Lutetium orthoborate has two stable structural modifications: vaterite forming at  $T = 750\text{--}850^\circ\text{C}$  and calcite forming at  $T = 970\text{--}1100^\circ\text{C}$ .  $\text{ReBO}_3$  ( $\text{Re} = \text{Gd}, \text{Tb}, \text{Eu}, \text{Y}$ ) orthoborates has a vaterite structure while  $\text{InBO}_3$  has a calcite structure [16–21].

In  $\text{Lu}_{0.98-x}\text{In}_x\text{Eu}_{0.02}\text{BO}_3$  orthoborate synthesized at  $T = 780^\circ\text{C}$  (the temperature of existence of the low-temperature  $\text{LuBO}_3$  vaterite) with increased In concentration, the following structural modification sequence (SMS) is observed: vaterite  $\rightarrow$  vaterite + calcite  $\rightarrow$  calcite.

These samples are crystallized in the calcite structure at  $\text{In} \geq 10$  at.% [15]. In  $\text{Lu}_{0.99-x}\text{Re}_x\text{Eu}_{0.01}\text{BO}_3$  ( $\text{Re} = \text{Eu}, \text{Gd}, \text{Tb}, \text{Y}$ ), synthesized at  $T = 970^\circ\text{C}$  (temperature of existence of the  $\text{LuBO}_3$  calcite phase) with increased  $\text{Re}$  concentration, the following SMS is observed: calcite  $\rightarrow$  calcite + vaterite  $\rightarrow$  vaterite.  $\text{Lu}_{0.99-x}\text{Re}_x\text{Eu}_{0.01}\text{BO}_3$  samples are crystallized in the vaterite structure at  $\text{Re} \geq 10\text{--}25$  at.% for different  $\text{Re}$  [11–14]. In luminescence spectra of  $\text{Lu}_{0.98-x}\text{In}_x\text{Eu}_{0.02}\text{BO}_3$  and  $\text{Lu}_{0.99-x}\text{Re}_x\text{Eu}_{0.01}\text{BO}_3$  samples having a calcite structure, two narrow bands with  $\lambda_{\text{max}} = 589.8$  and  $595.7$  nm (electronic transition  ${}^5D_0 \rightarrow {}^7F_1$ ) [8–15]. Vaterite modification luminescence spectrum of these compounds contains three bands: in  $588\text{--}596$  nm ( ${}^5D_0 \rightarrow {}^7F_1$ ),  $608\text{--}613$  and  $624\text{--}632$  nm ( ${}^5D_0 \rightarrow {}^7F_2$ ) regions [6–13]. Therefore,  $\text{Eu}^{3+}$  contained in the compounds and having a calcite and vaterite structure feature orange and red luminescence, respectively.

In luminescence spectrum of  $\text{LaBO}_3(\text{Eu})$  lanthanum orthoborate having an aragonite structure (space group  $Pnam$ ), bands with  $\lambda_{\text{max}} = 589.4, 591$  and  $592.6$  nm ( ${}^5D_0 \rightarrow {}^7F_1$ ) and some bands in the range of  $608\text{--}628$  nm ( ${}^5D_0 \rightarrow {}^7F_2$ ) have the highest intensity [22–25]. It is important that the spectral luminescence distribution of  $\text{LaBO}_3(\text{Eu})$  that has an aragonite structure is closer to the spectral luminescence distribution of  $\text{ReBO}_3(\text{Eu})$  that have a vaterite structure than to orthoborates that have a calcite structure.

The luminescence excitation spectra (LES) of the main luminescence bands of various structural modifications of  $ReBO_3(Eu)$  ( $Re = La, Gd, Eu, Y, Lu$ ) borates have wide bands (charge transfer bands (CTB)) in the ultraviolet spectrum, whose maximums for the aragonite, vaterite and calcite phases occur at  $\sim 283$ ,  $\sim 242$  and  $\sim 254$  nm, respectively. LES of these compounds also contain several narrow bands in the range of 290–500 nm corresponding to resonance excitation of  $Eu^{3+}$ . Bands  $\lambda_{ex} = 394$  nm ( ${}^7F_0 \rightarrow {}^5L_6$ ); 466.5, 469 nm ( ${}^7F_0 \rightarrow {}^5D_2$ ) are most intense in the long-wavelength region [3,9–12,22–25]. It should be also noted that the normalized intensities of the LES bands are close in orthoborates having the aragonite and vaterite structure, while, for the calcite structure, the intensity of the charge transfer band is significantly higher than that of the resonance bands. The presence of the dominant short-wavelength band is an important feature of the LES samples having the calcite structure.

It was shown for the first time in [26,27] that a band with  $\lambda_{ex} = 469$  nm ( ${}^7F_0 \rightarrow {}^5D_2$ ) in the luminescence excitation spectra (LES) and a band in the 577–582 nm ( ${}^5D_0 \rightarrow {}^7F_0$ ) region in the luminescence spectra of  $La_{0.99-x}Re_xEu_{0.01}BO_3$  ( $Re = Tb, Y$ ) may serve as structural state indicators for a sample. A band with  $\lambda_{ex} = 469$  nm is observed in LES of samples having a vaterite structure, while it is not observed in samples with an aragonite structure. In LS, if the maximum of the band corresponding to transition  ${}^5D_0 \rightarrow {}^7F_0$  occurs at wavelengths less than 580 nm, then the sample has an aragonite structure, if it occurs at  $\lambda$  greater than 580 nm, then the sample has a vaterite structure.

Structural and spectral characteristics of  $La_{0.99-x}Re_xEu_{0.01}BO_3$  ( $Re = Tb, Y$ ),  $La_{0.98-x}Lu_xEu_{0.02}BO_3$ ,  $Pr_{0.99-x}Lu_xEu_{0.01}BO_3$  and  $Lu_{0.99-x}Sm_xEu_{0.01}BO_3$  orthoborates synthesized at  $T = 970^\circ C$  are investigated in [22,26–29].  $LaBO_3$  and  $PrBO_3$  have two structural modifications. An orthorhombic phase — aragonite (space group  $Pnam$ ) is the low-temperature phase of these compounds. At  $T = 1488^\circ C$ ,  $LaBO_3$  transits to a high-temperature monoclinic phase (space group  $P2_1/m$ ), and  $PrBO_3$  at  $T = 1500^\circ C$  changes to a triclinic phase (space group  $P(-1)$ ) [30–35]. The triclinic structure (space group  $P(-1)$ ) is the low-temperature phase of  $SmBO_3$ , while at  $T = 1065–1150^\circ C$  (according to various publications),  $SmBO_3$  has a vaterite structure ( $P6_3/mmc$ ) [17,36–38].

It is worth to note that  $La^{3+}$  ions in the aragonite structure are surrounded by nine oxygen ions, while boron ions have a trigonal coordination by oxygen [32–35].  $Lu^{3+}$  ions in the calcite structure, e.g. in  $LuBO_3$ , are surrounded by six oxygen ions, while boron atoms have the same trigonal coordination by oxygen —  $(BO_3)^{3-}$  [39].  $Sm^{3+}$  ions in the triclinic structure of  $SmBO_3$  are surrounded by eight oxygen ions, while boron ions have a trigonal coordination by oxygen [36]. At the same time,  $Lu^{3+}$  ions in the vaterite structure are surrounded by eight oxygen ions, while three boron atoms with tetrahedral environment by oxygen make

up a  $(B_3O_9)^{9-}$  group in the form of a three-dimensional ring [39–41].

In  $La_{0.99-x}Re_xEu_{0.01}BO_3$  ( $Re = Tb, Y$ ) synthesized at  $T = 970^\circ C$  (temperature of existence of  $LaBO_3$  aragonite and  $ReBO_3$  vaterite phases), the following structural modification sequence (SMS) is observed with an increase in  $Re$  concentration: aragonite  $\rightarrow$  aragonite + vaterite  $\rightarrow$  vaterite [26,27]. At the same time, in  $La_{0.98-x}Lu_xEu_{0.02}BO_3$  and  $Pr_{0.99-x}Lu_xEu_{0.01}BO_3$  orthoborates synthesized at  $T = 970^\circ C$  (temperature of existence of  $LaBO_3$  and  $PrBO_3$  aragonite phases and  $LuBO_3$  calcite phases), an unexpected structural modification sequence is observed with an increase in  $Lu^{3+}$  concentration: aragonite  $\rightarrow$  aragonite + vaterite  $\rightarrow$  vaterite  $\rightarrow$  vaterite + calcite  $\rightarrow$  calcite [22,28].

In  $Lu_{0.99-x}Sm_xEu_{0.01}BO_3$  synthesized at  $T = 970^\circ C$  (temperature of existence of  $LuBO_3$  calcite phase and  $SmBO_3$  triclinic phase), gradual change of three structural states is also observed with an increase in  $Sm^{3+}$  concentration: calcite  $\rightarrow$  calcite + vaterite  $\rightarrow$  vaterite  $\rightarrow$  vaterite + triclinic phase  $\rightarrow$  triclinic phase [29]. This structural state sequence includes vaterite as an intermediate phase like in  $Re_{1-x}Lu_xBO_3(Eu)$  ( $Re = La, Pr$ ), synthesized at  $970^\circ C$ .

Thus, with an increase in  $Lu$  concentration in  $Re_{1-x}Lu_xBO_3(Eu)$  ( $Re = La, Pr$ ) and in  $Sm$  concentration in  $Lu_{1-x}Sm_xBO_3(Eu)$ , these compounds first form a vaterite phase from the aragonite and calcite phases which are equilibrium at the synthesis temperature and only then transit to a structure which is equilibrium at the synthesis temperature. It should be noted that the  $Sm^{3+}$  concentration range in which the vaterite phase exists in  $Lu_{0.99-x}Sm_xEu_{0.01}BO_3$  synthesized at  $970^\circ C$  is very wide  $0.3 \leq x \leq 0.95$ , while the triclinic phase exists in a very narrow range —  $0.98 < x \leq 1$  [29].

It is important to note that in  $Lu_{1-x}Re_xBO_3:Eu$ , ( $Re = Gd, Tb, Eu, Y$ ) and  $Lu_{1-x}In_xBO_3$  synthesized at  $970^\circ C$ , transition to the final structural modification takes place at  $In \geq 10$  at.% and  $Re \geq 10–25$  at.% (for different  $Re$ ) [11–15]. At the same time, in  $La_{0.99-x}Re_xEu_{0.01}BO_3$  ( $Re = Tb, Y$ ),  $La_{0.98-x}Lu_xEu_{0.02}BO_3$ ,  $Pr_{0.99-x}Lu_xEu_{0.01}BO_3$  and  $Lu_{0.99-x}Sm_xEu_{0.01}BO_3$  synthesized at  $T = 970^\circ C$ , this process is completed at  $x \geq 0.8–0.98$  (for different  $Re$ ) [22,26–29].

In [22,26–29], solid solutions of  $LaBO_3$  and  $ReBO_3$  rare-earth ion borates ( $Re = Tb, Y, Sm, Lu$ ) are studied. The investigation of solid solutions of  $LaBO_3$  and non-lanthanide borates is of interest. Solid solutions of  $LaBO_3$  and  $ScBO_3$  borates with general formula  $La_{0.99-x}Sc_xEu_{0.01}BO_3$  ( $0 \leq x \leq 0.99$ ) are studied herein.

Scandium orthoborate ( $ScBO_3$ ) is known to have one structural modification — calcite [17,19,42]. However, [43] shows that a vaterite phase is formed when amorphous precursor  $ScBO_3$  is annealed first in a narrow temperature range  $710–730^\circ C$ , and a calcite phase is observed at temperatures higher than  $740^\circ C$ .

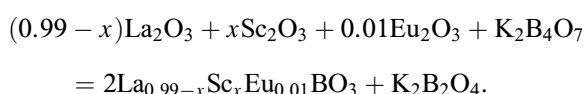
Structure, IR spectra, morphology, luminescence spectra and luminescence excitation spectra of  $Lu_{0.99-x}Sc_xEu_{0.01}BO_3$  at  $0 \leq x \leq 0.99$  are investigated

herein. The correspondence between structure and spectral characteristics of these compounds is established.  $\text{Eu}^{3+}$  ions, like in our previous investigations, were used as optically active and structure-sensitive labels in amounts not affecting the structural transformations of orthoborates.

## 2. Experimental procedures

### 2.1. Synthesis of samples

Polycrystalline powder samples of  $\text{La}_{0.99-x}\text{Sc}_x\text{Eu}_{0.01}\text{BO}_3$  were synthesized at  $0 \leq x \leq 0.99$  by interaction of lanthanum, scandium and europium oxides with potassium tetraborate melt according to reaction



The amount of potassium tetraborate taken for the reaction provided an excess of the boron-containing reagent with respect to the stoichiometric amount by 10–20%.  $\text{K}_2\text{B}_4\text{O}_7 \cdot 4\text{H}_2\text{O}$ , metal oxides and nitric acid were used as precursor for the synthesis. All chemicals were of „analytical reagent grade“. Metal ions were reacted in the form of aqueous solutions of their nitrate salts obtained by dissolution of initial metal oxides in nitric acid. Microcrystalline borate powders were synthesized as follows. Accurately weighed crystalline potassium tetraborate (hydrate) and appropriate volumes of calibrated aqueous solutions of rare earth nitrates were placed in a ceramic cup and mixed thoroughly. The obtained aqueous suspension was heated on a hot plate with water distilled off at a moderate boil. The resulting solid product was annealed at  $550^\circ\text{C}$  during 20 min to remove any residual moisture and to decompose the nitrate salts. The solid precursor product was carefully ground in an agate mortar and then the resulting powder was placed in a ceramic for annealing at  $T = 970^\circ\text{C}$  during 3 h. The derived products were treated with 5 wt.% aqueous solution of hydrochloric acid during 0.2 h. Borate polycrystals were extracted by filtering the obtained aqueous suspension, followed by washing with water and alcohol and drying on the filter. The obtained polycrystal powders were finally air dried at  $T = 120^\circ\text{C}$  during 0.5 h.

### 2.2. Research methods

X-ray diffraction examinations were performed using a Rigaku SmartLab SE diffractometer with  $\text{CuK}_\alpha$ -radiation,  $\lambda = 1.54178 \text{ \AA}$ , 40 kV, 35 mA. Angular spacing is  $2\theta = 10\text{--}140^\circ$ . Phase analysis of the samples and calculation of lattice parameters were performed using Match and PowderCell 2.4 software.

IR absorption spectra were measured using VERTEX 80v Fourier spectrometer in a spectral range from 400 to  $5000 \text{ cm}^{-1}$  with resolution  $2 \text{ cm}^{-1}$ . For measurements, the polycrystal powders were ground in the agate mortar, and

then applied in a thin layer onto a polished KBr crystalline substrate.

The sample morphology was examined using Supra 50VP X-ray microanalyzer with INCA EDS accessory (Oxford).

Photoluminescence spectra and luminescence excitation spectra were studied using a unit consisting of a light source — DKSSh-150 lamp, two MDR-4 and MDR-6 monochromators (spectral range from 200 to 1000 nm, dispersion —  $1.3 \text{ nm/mm}$ ). Luminescence was recorded by means of FEU-106 photomultiplier (spectral sensitivity range from 200 to 800 nm) and an amplification system. MDR-4 monochromator was used to study the luminescence excitation spectra of the samples, MDR-6 monochromator was used to study luminescence spectra. Spectral and structural characteristics as well as morphology of the samples were studied at room temperature.

## 3. X-ray diffraction examinations

Diffraction patterns of  $\text{La}_{0.99-x}\text{Sc}_x\text{Eu}_{0.01}\text{BO}_3$  sample powders and their phase composition depending on the mole ratio of lanthanum and scandium in the charge with  $0 \leq x \leq 0.99$  are shown in Figures 1 and 2. With  $0 \leq x \leq 0.26$ , the samples are single-phase and have an  $\text{LaBO}_3$  aragonite structure, space group  $Pnam$  (62) (PDF 12-0762),  $Z = 4$ . With  $0.26 < x < 0.75$ , the samples are two-phase — besides the aragonite structure, trigonal phase  $\text{LaSc}_3(\text{BO}_3)_4$ , space group  $R32H$  (155),  $Z = 3$  (huntite structure) was observed [44]. With further increase in  $\text{Sc}^{3+}$  concentration, relative amount of huntite grows, while relative amount of aragonite decreases. With  $0.75 \leq x \leq 0.85$ ,  $\text{LaSc}_3(\text{BO}_3)_4$  lanthanum–scandium borate is observed that is known to have 3 crystalline modifications: trigonal (space group  $R32$ ) and two monoclinic (space group  $C2/c$  and  $Cc$ ) [44,45].  $\text{La}_{0.24}\text{Sc}_{0.75}\text{Eu}_{0.01}\text{BO}_3$  samples contain  $\sim 98.5\%$  of the trigonal phase, space group  $R32H$  and  $\sim 1.5\%$  of the monoclinic phase, space group  $C2/c$  (15) (PDF 051-0106),  $Z = 4$ .  $\text{La}_{0.14}\text{Sc}_{0.85}\text{Eu}_{0.01}\text{BO}_3$  sample has a trigonal structure, space group  $R32H$ . With  $0.85 < x \leq 0.97$ , the samples are two-phase and contain  $\text{LaSc}_3(\text{BO}_3)_4$  huntite and  $\text{ScBO}_3$  calcite, space group  $R\bar{3}c$  (167), PDF 79-0097,  $Z = 6$ . With further increase in  $\text{Sc}^{3+}$  concentration, amount of calcite grows, while amount of huntite decreases.  $\text{Sc}_{0.99}\text{Eu}_{0.01}\text{BO}_3$  sample contains  $\sim 97\%$  of calcite and  $\sim 3\%$  of  $\text{Sc}_2\text{O}_3$  (PDF 05-0629). It should be noted that in samples containing 31, 37, 48, 60, 70, 85, 90, 95 and 97 at.% of  $\text{Sc}^{3+}$ , the existing huntite phase has a trigonal structure (space group  $R32H$ ). Thus, with an increase in  $\text{Sc}^{3+}$  concentration in  $\text{La}_{0.99-x}\text{Sc}_x\text{Eu}_{0.01}\text{BO}_3$  samples synthesized at  $970^\circ\text{C}$ , three compounds are formed gradually — lanthanum orthoborate, lanthanum — scandium borate  $\text{LaSc}_3(\text{BO}_3)_4$ ,  $\text{ScBO}_3$  scandium orthoborate.

Figure 3 shows the volumes of lattice cells observed in  $\text{La}_{0.99-x}\text{Sc}_x\text{Eu}_{0.01}\text{BO}_3$  at  $0 \leq x \leq 0.99$  reduced to  $(\text{La}, \text{Sc})\text{BO}_3$  formula unit. When scandium concentrations

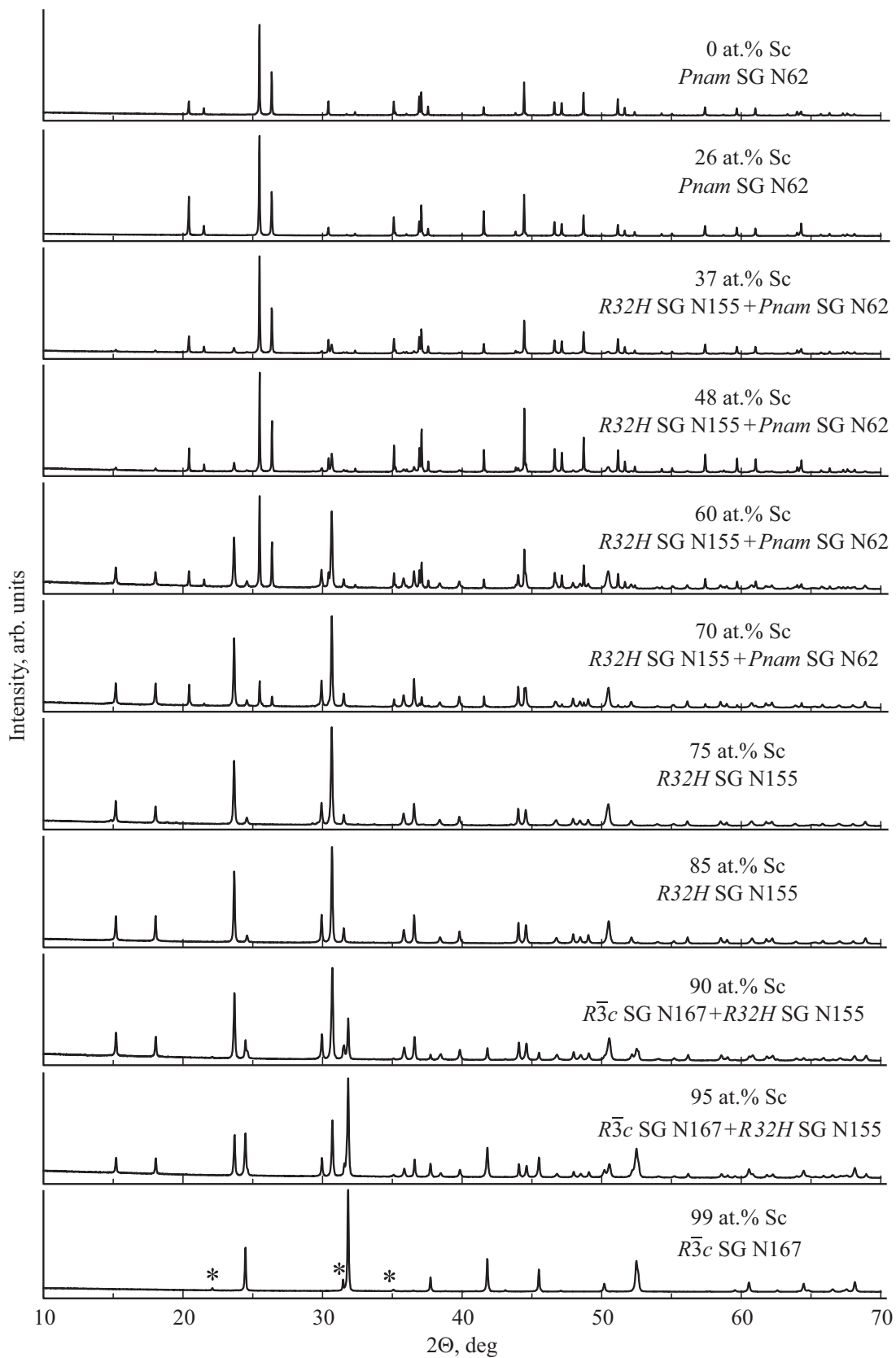


**Figure 1.** Diffraction patterns of  $\text{La}_{0.99-x}\text{Sc}_x\text{Eu}_{0.01}\text{BO}_3$  ( $0 \leq x \leq 0.99$ ) samples.

Phase content and lattice cell volume reduced to  $(\text{La,Sc})\text{BO}_3$  formula unit, for  $\text{LaBO}_3$  ( $V_A$ ) aragonite,  $\text{LaSc}_3(\text{BO}_3)_4$  ( $V_H$ ) huntite and  $\text{ScBO}_3$  ( $V_C$ ) calcite depending on the scandium content in  $\text{La}_{0.99-x}\text{Sc}_x\text{Eu}_{0.01}\text{BO}_3$  charge

Sc, at.% in the charge	Aragonite, % space group $Pnam$	$V_A, \text{\AA}^3$	Huntite, % space group $R32H$	$V_H, \text{\AA}^3$	Calcite, % space group $R\bar{3}c$	$V_C, \text{\AA}^3$
0	100	61.80	0	—	0	—
15	100	61.80	0	—	0	—
26	100	61.79	0	—	0	—
31	82	61.78	18	—	0	—
37	73	61.79	27	55.66	0	—
48	54	61.75	46	55.67	0	—
60	22	61.74	78	55.64	0	—
70	7	61.66	93	55.59	0	—
<sup>1)</sup> 75	0	—	~ 100	55.53	0	—
85	0	—	100	55.51	0	—
90	0	—	65	55.29	35	50.03
95	0	—	26	55.30	74	50.11
97	0	—	13	55.25	87	50.14
<sup>2)</sup> 99	0	—	0	—	~ 100	50.16

Note. <sup>1)</sup>  $\text{La}_{0.24}\text{Sc}_{0.75}\text{Eu}_{0.01}\text{BO}_3$  sample contains ~ 98.5% of the trigonal phase, space group  $R32H$  and ~ 1.5% of monoclinic phase, space group  $C2/c$ .  
<sup>2)</sup>  $\text{Sc}_{0.99}\text{Eu}_{0.01}\text{BO}_3$  sample contains ~ 97% of calcite and ~ 3% of  $\text{Sc}_2\text{O}_3$ .

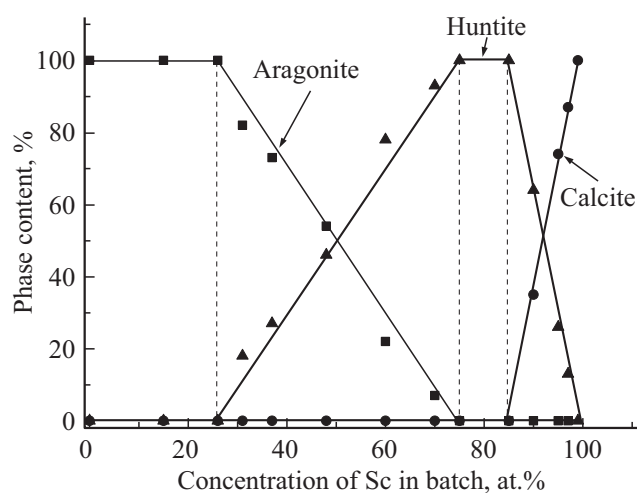


**Figure 2.** Phase composition of  $\text{La}_{0.99-x}\text{Sc}_x\text{Eu}_{0.01}\text{BO}_3$  depending on the rare earth ratio in the charge with  $0 \leq x \leq 0.99$ : square —  $\text{La}_{0.99-x}\text{Eu}_{0.01}\text{BO}_3$  aragonite, triangle —  $\text{La}_{0.99}\text{Sc}_3\text{Eu}_{0.01}(\text{BO}_3)_4$  huntite, circle —  $\text{Sc}_{0.99}\text{Eu}_{0.01}\text{BO}_3$  calcite.

in the charge are  $0 \leq x \leq 0.26$  in a single-phase sample, the aragonite lattice cell volume ( $V_A$ ) is unchanged (Table, Figure 3). When  $\text{La}^{3+}$  are substituted with  $\text{Sc}^{3+}$ , obvious decrease in  $V_A$  would have been observed, because the ionic radius of  $\text{Sc}^{3+}$  (0.73438 Å) is 1.5 as small as the ionic radius of  $\text{La}^{3+}$  (1.11482 Å) [46]. Uniformity of  $V_A$  proves that  $\text{Sc}^{3+}$  ions are not included in  $\text{LaBO}_3$  structure, when their mole content in the charge is up to 26%. This conclusion is also supported by the fact that with  $0 \leq x \leq 0.26$  diffraction patterns of  $\text{La}_{0.99-x}\text{Sc}_x\text{Eu}_{0.01}\text{BO}_3$  contain only the lines specific to  $\text{La}_{0.99}\text{Eu}_{0.01}\text{BO}_3$  aragonite structure and no diffraction line displacement of aragonite phase is

observed (Figure 4, a). To check whether there is any diffraction line displacement, non-overlapping lines (111) for aragonite and (021) for huntite were selected. According to the microprobe elemental analysis, the products not subjected to acid treatment contain scandium, while these compounds treated with aqueous solution of hydrochloric acid contain no scandium. Thus, it can be suggested that with  $0 \leq x \leq 0.26$  scandium is not included in the crystalline structure of  $\text{LaBO}_3$ , but rather forms an acid-soluble amorphous compound with boron-containing reaction products.

With  $0.26 < x < 0.75$ , a slight decrease in the aragonite cell volume and a slight line displacement of aragonite into

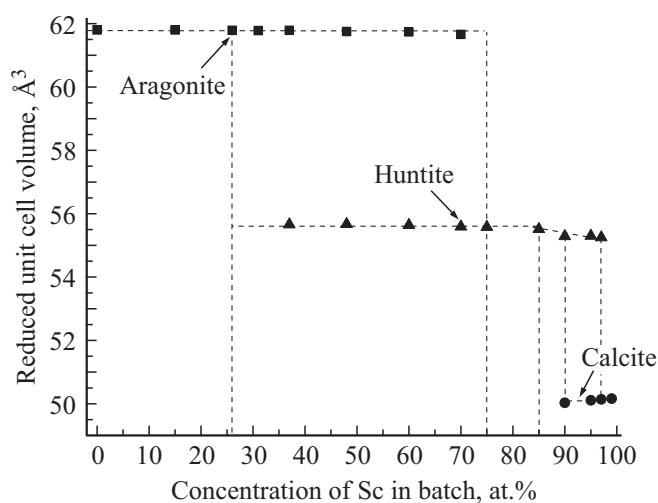


**Figure 3.** Volumes of aragonite, huntite and calcite lattice cells depending on rare earth ratio in the charge with  $0 \leq x \leq 0.99$  reduced to  $(\text{La,Sc})\text{BO}_3$  formula unit: square — aragonite, triangle — huntite, circle — calcite.

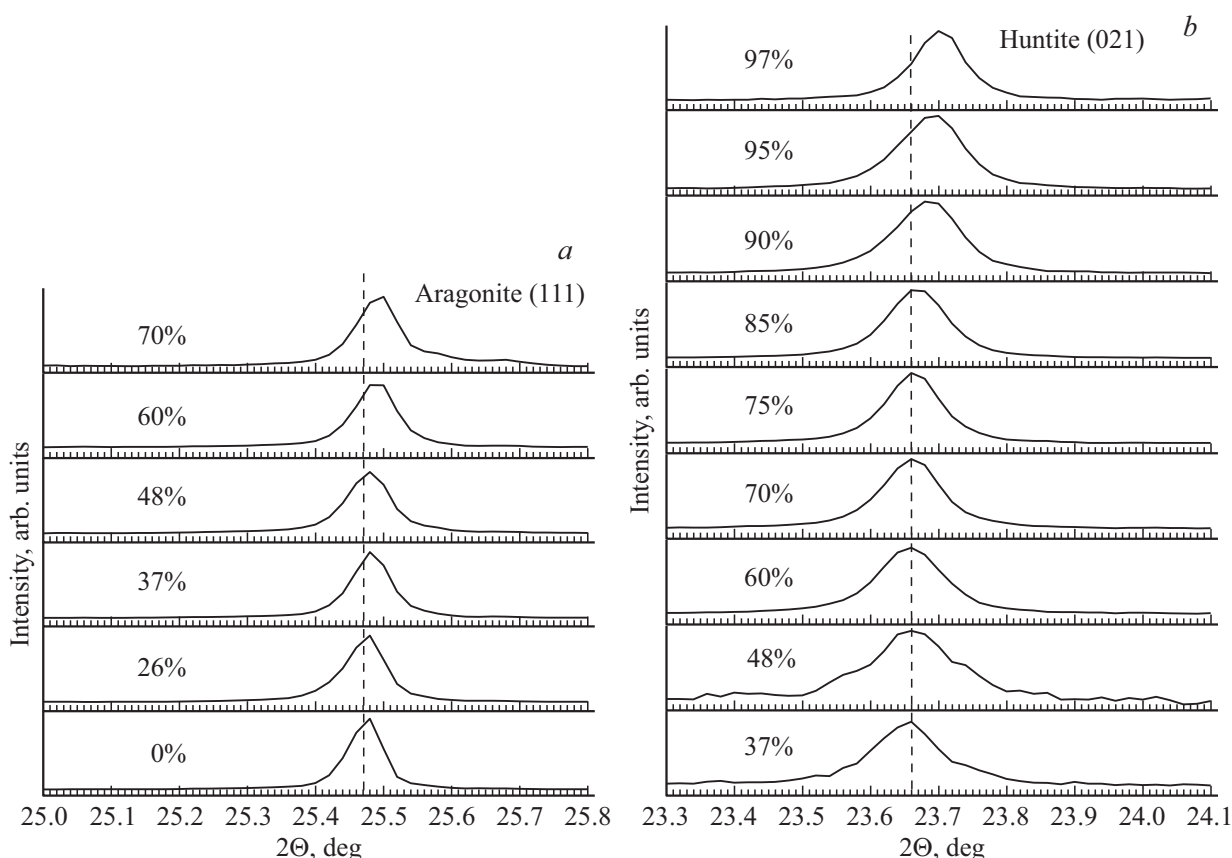


**Figure 4.** Position of diffraction lines of  $\text{La}_{0.99-x}\text{Sc}_x\text{Eu}_{0.01}\text{BO}_3$  with different Sc concentrations in the charge: *a* — line of (111) aragonite phase  $\text{La}_{0.99-x}\text{Eu}_{0.01}\text{BO}_3$ , *b* — line of (021) huntite phase  $\text{La}_{0.99}\text{Sc}_3\text{Eu}_{0.01}(\text{BO}_3)_4$ .

a larger angle region (Figure 3; 4, *a*) is observed suggesting that a small amount of  $\text{La}^{3+}$  is substituted with  $\text{Sc}^{3+}$ . At the same time, in this  $\text{Sc}^{3+}$  concentration range, the cell volume of  $\text{LaSc}_3(\text{BO}_4)_3$  ( $V_H$ ) huntite remains almost the same and line positions of this phase is not changed (Figure 3; 4, *b*). In the scandium concentration range  $0.75 \leq x \leq 0.85$  where  $\text{LaSc}_3(\text{BO}_4)_3$  huntite is observed, the lattice cell volume  $V_H$  and position of (021) lines are unchanged (Figure 3; 4, *b*). With  $0.85 < x \leq 0.97$ ,  $\text{LaSc}_3(\text{BO}_4)_3$  cell volume is slightly decreased. Diffraction lines of the huntite phase are displaced into a larger angle region (Figure 3; 4, *b*) suggesting that a small amount of  $\text{La}^{3+}$  is substituted with  $\text{Sc}^{3+}$  and the volume of  $\text{LaSc}_3(\text{BO}_4)_3$  lattice cell is decreased. In the scandium concentration region  $0.85 < x \leq 0.99$ , the volume of  $\text{ScBO}_3$  calcite lattice cell is virtually unchanged. (Figure 3, Table).

According to the X-ray diffraction examinations of compounds with general formula  $\text{La}_{0.99-x}\text{Sc}_x\text{Eu}_{0.01}\text{BO}_3$  at  $0 \leq x \leq 0.99$ , a conclusion may be made that with an increase in  $\text{Sc}^{3+}$  concentration in the charge, gradual change of three types of structural states is observed: aragonite  $\text{LaBO}_3$  ( $0 \leq x \leq 0.26$ ) → aragonite + huntite  $\text{LaSc}_3(\text{BO}_4)_3$  ( $0.26 < x < 0.75$ ) → huntite ( $0.75 \leq x \leq 0.85$ ) → huntite + calcite  $\text{ScBO}_3$  ( $0.85 < x \leq 0.97$ ) → calcite ( $0.97 < x \leq 0.99$ ).

Special attention shall be paid to the fact that with increase of  $x$  another compound is formed in  $\text{La}_{0.99-x}\text{Sc}_x\text{Eu}_{0.01}\text{BO}_3$  samples, besides  $\text{LaBO}_3$  and  $\text{ScBO}_3$  —  $\text{LaSc}_3(\text{BO}_3)_4$  lanthanum-scandium borate. At the same time, only orthoborates are formed in  $\text{La}_{0.99-x}\text{Re}_x\text{Eu}_{0.01}\text{BO}_3$  ( $\text{Re} = \text{Tb}, \text{Y}, \text{Lu}$ ) compounds studied before when  $\text{Re}^{3+}$  concentration is increased:  $\text{La}_{0.99}\text{Eu}_{0.01}\text{BO}_3$ ,  $\text{La}_{0.99-x}\text{Re}_x\text{Eu}_{0.01}\text{BO}_3$  and  $\text{Re}_{0.99}\text{Eu}_{0.01}\text{BO}_3$  [22,26,27].

#### 4. Morphology of samples

In  $\text{La}_{0.99-x}\text{Sc}_x\text{Eu}_{0.01}\text{BO}_3$  in concentration range  $\text{Sc}^{3+}$   $0 \leq x \leq 0.26$  having an aragonite structure (Table) according to the X-ray diffraction analysis, mostly microcrystals with size  $\sim 1-6 \mu\text{m}$  are observed (Figure 5, *a, b*).  $\text{La}_{0.62}\text{Sc}_{0.37}\text{Eu}_{0.01}\text{BO}_3$  samples (73% of  $\text{La}_{0.99}\text{Eu}_{0.01}\text{BO}_3$  aragonite (A) and 27% of  $\text{La}_{0.99}\text{Sc}_3\text{Eu}_{0.01}(\text{BO}_3)_4$  huntite (H), Table) contain, besides those mentioned above, elongated microcrystals in the form of well faceted columns whose opposite ends are pyramidal (Figure 5, *c*). With further increase in  $\text{Sc}^{3+}$  concentration, the number of „columnar“ microcrystals grows (Figure 5, *d*). In  $\text{La}_{0.24}\text{Sc}_{0.75}\text{Eu}_{0.01}\text{BO}_3$  and  $\text{La}_{0.14}\text{Sc}_{0.85}\text{Eu}_{0.01}\text{BO}_3$  samples containing 100% of huntite, „columnar“

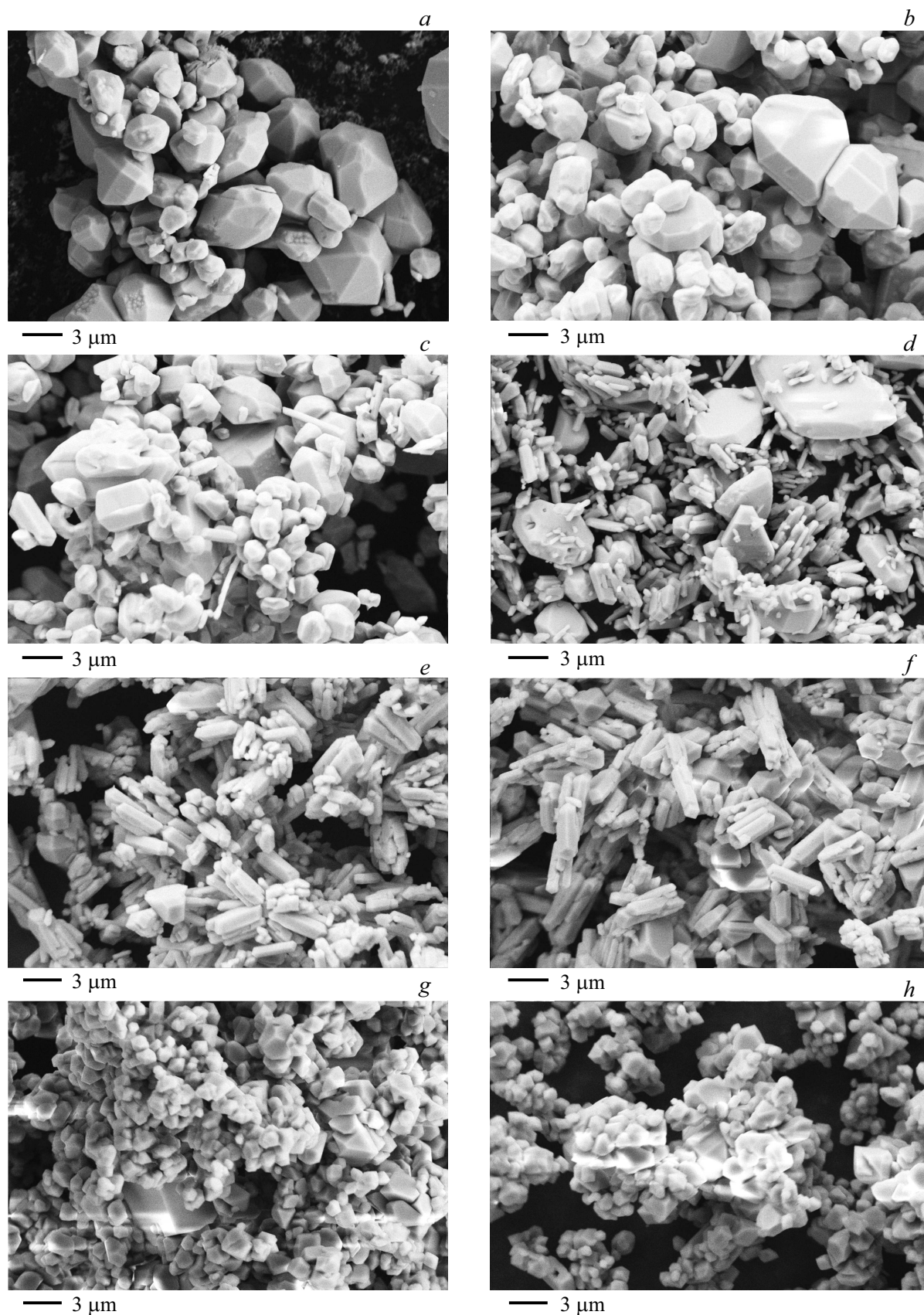


**Figure 5.** Morphology of borates  $\text{La}_{0.99-x}\text{Sc}_x\text{Eu}_{0.01}\text{BO}_3$  *a* —  $\text{La}_{0.84}\text{Sc}_{0.15}\text{Eu}_{0.01}\text{BO}_3$ ; *b* —  $\text{La}_{0.73}\text{Sc}_{0.26}\text{Eu}_{0.01}\text{BO}_3$ ; *c* —  $\text{La}_{0.62}\text{Sc}_{0.37}\text{Eu}_{0.01}\text{BO}_3$ ; *d* —  $\text{La}_{0.39}\text{Sc}_{0.6}\text{Eu}_{0.01}\text{BO}_3$ ; *e* —  $\text{La}_{0.14}\text{Sc}_{0.85}\text{Eu}_{0.01}\text{BO}_3$ ; *f* —  $\text{La}_{0.09}\text{Sc}_{0.9}\text{Eu}_{0.01}\text{BO}_3$ ; *g* —  $\text{La}_{0.02}\text{Sc}_{0.97}\text{Eu}_{0.01}\text{BO}_3$ ; *h* —  $\text{Sc}_{0.99}\text{Eu}_{0.01}\text{BO}_3$ .

microcrystals  $0.3\text{--}1 \times 1\text{--}4\ \mu\text{m}$  in size are primarily observed (Figure 5, *e*).  $\text{La}_{0.09}\text{Sc}_{0.9}\text{Eu}_{0.01}\text{BO}_3$  samples (65% of (*H*) and 35% of calcite  $\text{Sc}_{0.99}\text{Eu}_{0.01}\text{BO}_3$  (*C*)), besides „columnar“ microcrystals, contain microcrystals  $1\text{--}4\ \mu\text{m}$  in size (Figure 5, *f*). With further increase in  $\text{Sc}^{3+}$  concentration, the number of „columnar“ microcrystals decreases. In  $\text{La}_{0.02}\text{Sc}_{0.97}\text{Eu}_{0.01}\text{BO}_3$  samples (13% of *H* and 87% of *C*), primarily microcrystals  $1\text{--}3\ \mu\text{m}$  in size and a small amount of larger microcrystals  $4\text{--}5\ \mu\text{m}$  in size are observed (Figure 5, *g*).  $\text{Sc}_{0.99}\text{Eu}_{0.01}\text{BO}_3$  orthoborates having a calcite structure contain microcrystals  $1\text{--}3\ \mu\text{m}$  in size (Figure 5, *h*).

Morphology study of  $\text{La}_{0.99-x}\text{Sc}_x\text{Eu}_{0.01}\text{BO}_3$  ( $0 \leq x \leq 0.99$ ) borates suggests that  $\text{La}_{0.99}\text{Sc}_3\text{Eu}_{0.01}(\text{BO}_3)_4$  samples having a huntite structure contain well faceted columns  $0.3\text{--}1 \times 1\text{--}4\ \mu\text{m}$  in size with pyramidal opposite ends (Figure 5, *e*).  $\text{La}_{0.99}\text{Eu}_{0.01}\text{BO}_3$  orthoborates having an aragonite structure contain microcrystals  $1\text{--}6\ \mu\text{m}$  in size (Figure 5, *a*), and the size of  $\text{Sc}_{0.99}\text{Eu}_{0.01}\text{BO}_3$  microcrystals having a calcite structure is equal to  $1\text{--}3\ \mu\text{m}$  (Figure 5, *h*).

## 5. Results of IR-spectroscopy

Figure 6 shows IR spectra of  $\text{La}_{0.99-x}\text{Sc}_x\text{Eu}_{0.01}\text{BO}_3$  orthoborates at  $0 \leq x \leq 0.99$  in the frequency range of internal vibrations of the B-O bonds. In spectra of  $\text{La}_{0.99}\text{Eu}_{0.01}\text{BO}_3$  and  $\text{La}_{0.73}\text{Sc}_{0.26}\text{Eu}_{0.01}\text{BO}_3$  samples, absorption bands 593, 613, 723, 789, 940 and  $1306\ \text{cm}^{-1}$  marked as „a“ (Figure 6, spectra 1, 2). According to the X-ray diffraction analysis, these samples crystallize in the aragonite lattice (Table). In the aragonite structure, each boron atom is surrounded by three oxygen atoms and forms a planar ion  $(\text{BO}_3)^{3-}$  with positional symmetry  $C_s$ . According to the internal vibrations analysis of this ion in the aragonite structure [47], IR absorption bands 592 and  $613\ \text{cm}^{-1}$  may be attributed to bending in-plane vibration  $\nu_4$ , doublet 723, 789 may be attributed to bending out-of-plane vibration  $\nu_2$ , and the absorption bands 940 and  $1306\ \text{cm}^{-1}$  may be attributed to symmetric  $\nu_1$  and asymmetric  $\nu_3$  stretching vibrations, respectively (Fig. 6, spectrum 1). Similar spectra were observed in [48,34]. In spectra of  $\text{La}_{0.99-x}\text{Sc}_x\text{Eu}_{0.01}\text{BO}_3$  samples containing 31, 37, 48, 60, 70 at.%  $\text{Sc}^{3+}$ , along with bands „a“, new bands occur which are marked as „t“ (Figure 6, spectra 3–6). These samples are two-phase — besides  $\text{LaBO}_3$  aragonite phase, they contain  $\text{LaSc}_3(\text{BO}_3)_4$  aragonite phase, space group  $R32H$  (Table).

Crystalline structure with general formula  $\text{ReM}_3(\text{BO}_3)_4$ , where  $\text{Re} = \text{La}\text{--}\text{Lu}$ ,  $Y$ ;  $\text{M} = \text{Al}$ ,  $\text{Ga}$ ,  $\text{Cr}$ ,  $\text{Fe}$ ,  $\text{Sc}$  belongs to the structural type of  $\text{CaMg}_3(\text{BO}_3)_4$  huntite mineral which crystallizes in a trigonal structure and belongs to space group  $R32$ . Compared with calcite, the huntite structure includes two types of  $\text{BO}_3$  groups in the form of equilateral triangles with symmetry  $D_3$  and isosceles triangles with symmetry  $C_2$  [49,50]. A factor group analysis of internal vibrations of  $(\text{BO}_3)^{3-}$  in this structure and

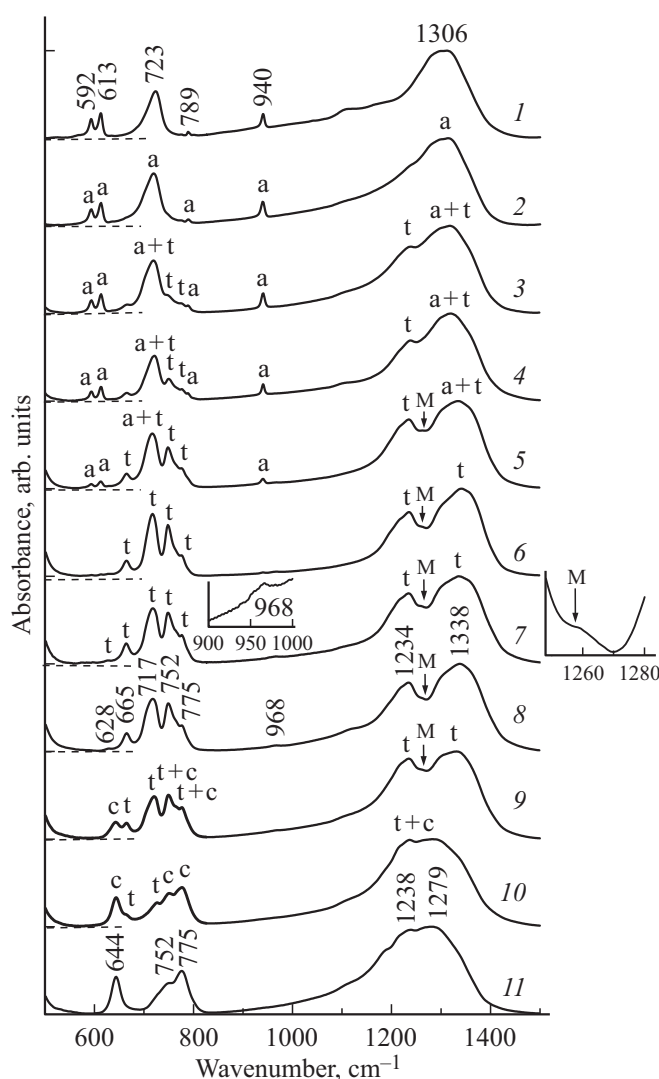


**Figure 6.** IR spectra of borates  $\text{La}_{0.99-x}\text{Sc}_x\text{Eu}_{0.01}\text{BO}_3$ : 1 —  $\text{La}_{0.99}\text{Eu}_{0.01}\text{BO}_3$ ; 2 —  $\text{La}_{0.73}\text{Sc}_{0.26}\text{Eu}_{0.01}\text{BO}_3$ ; 3 —  $\text{La}_{0.62}\text{Sc}_{0.37}\text{Eu}_{0.01}\text{BO}_3$ ; 4 —  $\text{La}_{0.51}\text{Sc}_{0.48}\text{Eu}_{0.01}\text{BO}_3$ ; 5 —  $\text{La}_{0.39}\text{Sc}_{0.6}\text{Eu}_{0.01}\text{BO}_3$ ; 6 —  $\text{La}_{0.29}\text{Sc}_{0.7}\text{Eu}_{0.01}\text{BO}_3$ ; 7 —  $\text{La}_{0.24}\text{Sc}_{0.75}\text{Eu}_{0.01}\text{BO}_3$ ; 8 —  $\text{La}_{0.14}\text{Sc}_{0.85}\text{Eu}_{0.01}\text{BO}_3$ ; 9 —  $\text{La}_{0.09}\text{Sc}_{0.9}\text{Eu}_{0.01}\text{BO}_3$ ; 10 —  $\text{La}_{0.04}\text{Sc}_{0.95}\text{Eu}_{0.01}\text{BO}_3$ ; 11 —  $\text{Sc}_{0.99}\text{Eu}_{0.01}\text{BO}_3$ . For spectra 1–10, zero values of the y axes are shown by a dotted line. The insert shows scaled-up spectrum regions in  $900\text{--}1000$  and  $1250\text{--}1280\ \text{cm}^{-1}$  ranges on the x and y axes.

investigation of IR spectra of  $\text{ReM}_3(\text{BO}_3)_4$  borates are described in [51]. In accordance with selection rules for IR spectra of compounds with space group  $R32$  and two types of  $(\text{BO}_3)^{3-}$  ions, the following are allowed: one band of vibrations  $\nu_1$  ( $E$ ), three bands of vibrations  $\nu_2$  ( $2A_2 + E$ ) and four vibrations  $\nu_3$  and  $\nu_4$  ( $A_2 + 3E$ ) each [51].

IR spectra of  $\text{La}_{0.24}\text{Sc}_{0.75}\text{Eu}_{0.01}\text{BO}_3$  and  $\text{La}_{0.14}\text{Sc}_{0.85}\text{Eu}_{0.01}\text{BO}_3$  samples having  $R32H$  structure contain only absorption bands „t“: 630, 665, 717, 752, 775, 968, 1234, 1238 (Figure 6, spectra 6, 7). According to IR spectra analysis of  $\text{ReM}_3(\text{BO}_3)_4$  compounds with

trigonal modification *R32H* described in [51–55], two wide intense bands with crests 1234 and 1338  $\text{cm}^{-1}$  in the frequency range  $\sim 1200\text{--}1400\text{ cm}^{-1}$  may be assigned to asymmetric B-O stretching vibrations  $\nu_3$  of  $(\text{BO}_3)^{3-}$  in two independent positions in the structure: with positional symmetry  $D_3$  and  $C_2$ , respectively; several bands in range  $\sim 610\text{--}800\text{ cm}^{-1}$  may be assigned to bending vibrations  $\nu_4$  and  $\nu_2$ , and weak band  $\sim 968\text{ cm}^{-1}$  may be assigned to symmetrical vibration  $\nu_1$ .

Comparison between IR spectra of  $\text{La}_{0.99}\text{Eu}_{0.01}\text{BO}_3$  samples having the aragonite structure and  $\text{La}_{0.24}\text{Sc}_{0.75}\text{Eu}_{0.01}\text{BO}_3$  and  $\text{La}_{0.14}\text{Sc}_{0.85}\text{Eu}_{0.01}\text{BO}_3$  samples having trigonal structure *R32H* shows that: strong vibration absorption band  $\nu_3$  1306  $\text{cm}^{-1}$  in the aragonite structure is within vibration frequency range  $\nu_3$  of trigonal structure *R32H*, intense bending vibration frequency 723  $\text{cm}^{-1}$  of the aragonite phase is very close to vibration frequency 717  $\text{cm}^{-1}$  of  $\text{LaSc}_3(\text{BO}_3)_4$  phase, and vibration absorption strength  $\nu_1$  (968  $\text{cm}^{-1}$ ) in *R32H* phase is very weak compared with  $\nu_1$  (940  $\text{cm}^{-1}$ ) in the aragonite phase.

The X-ray diffraction analysis shows that the amount of aragonite phase decreases and the amount of trigonal phase increases in  $\text{Lu}_{0.99-x}\text{Sc}_x\text{Eu}_{0.01}\text{BO}_3$  ( $0.31 \leq x \leq 0.7$ ) samples with an increase in Sc concentration (Table). This change in the phase ratio is fully compliant with the changes in absorption band intensities in IR spectra — intensities of bands „a“ decrease, while that of bands „t“ increase (Figure 6, spectra 3–6).

As described in Section 3,  $\text{La}_{0.24}\text{Sc}_{0.75}\text{Eu}_{0.01}\text{BO}_3$  sample contains 98.5% of the trigonal phase, space group *R32H* and 1.5% of monoclinic phase, space group *C2/c* (Figure 1, Table). It has been found earlier that  $\text{ReAl}_3(\text{BO}_3)_4$  rare earth borates, where  $\text{R} = \text{Y, Nd–Yb}$ , may have rhombohedral structure *R32* and monoclinic modifications *C2/c* and *C2* close to it [56,57]. These compounds are of polytype nature distinguished by the presence of fragments with different type of ordering [58]. Possible similar polytype structures are expected for lanthanum-scandium borates [50]. It is shown in [54] that IR spectrum of  $\text{YAl}_3(\text{BO}_3)_4$  with *R32* structure has a band  $\sim 1310\text{ cm}^{-1}$  in the form of an shoulder which is characteristic to IR spectra of monoclinic phase *C2/c*. Similar weak absorption band  $\sim 1260\text{ cm}^{-1}$ , marked as M is observed in the spectrum of  $\text{La}_{0.24}\text{Sc}_{0.75}\text{Eu}_{0.01}\text{BO}_3$  sample (Figure 7 spectrum 7, insert) with trigonal structure *R32H*. This may be caused by the presence of monoclinic phase fragments in the trigonal structure of  $\text{La}_{0.24}\text{Sc}_{0.75}\text{Eu}_{0.01}\text{BO}_3$  sample. This band is also observed in IR spectra of other samples (Figure 7 spectra 5, 6, 8, 9). However, diffraction patterns of these samples contain no monoclinic phase reflections (Figure 1), which may be associated with a lower content of the monoclinic phase in these samples.

In IR spectra of  $\text{Sc}_{0.99}\text{Eu}_{0.01}\text{BO}_3$  sample containing  $\sim 97\%$  of calcite and  $\sim 3\%$  of  $\text{Sc}_2\text{O}_3$ , absorption bands 644, 752, 775, 1236 and 1279  $\text{cm}^{-1}$  („c“) are observed which are caused by internal B-O stretching vibrations of trigonal

$(\text{BO}_3)^{3-}$  ion with local symmetry  $D_3$  (Figure 6, spectrum 11). Similar spectrum has been observed earlier in borates with calcite structure [12,15,48]. Band 644 and doublet 752 and 775  $\text{cm}^{-1}$  are assigned to asymmetric and symmetric B-O bending vibrations —  $\nu_4$  and  $\nu_2$ , respectively, and wide band 1200–1400  $\text{cm}^{-1}$  with maximums 1236 and 1279  $\text{cm}^{-1}$  is assigned to asymmetric B-O stretching vibrations.

In IR spectra of two-phase  $\text{La}_{0.09}\text{Sc}_{0.90}\text{Eu}_{0.01}\text{BO}_3$  and  $\text{La}_{0.04}\text{Sc}_{0.95}\text{Eu}_{0.01}\text{BO}_3$  samples containing a trigonal phase and calcite phase (Table), absorption bands specific to these structures — „t“ are „c“ are observed (Figure 6, spectra 9, 10). According to the phase composition of these samples, absorption band intensity of the trigonal phase decreases and absorption band intensity of calcite increases with an increase in  $\text{Sc}^{3+}$  concentration.

Therefore, the IR spectroscopy examination of  $\text{La}_{0.99-x}\text{Sc}_x\text{Eu}_{0.01}\text{BO}_3$  ( $0 \leq x \leq 0.99$ ) system has shown that, with growth of  $\text{Sc}^{3+}$  concentration in the frequency region of B-O stretching vibrations of  $\text{BO}_3$  trigonal groups, vibration spectrum of samples changes and well-defined correspondence is observed between the IR spectra and structural state of samples. While the coordination number of boron remains unchanged as opposed, for example, to  $\text{La}_{0.98-x}\text{Lu}_{1-x}\text{Eu}_{0.02}\text{BO}_3$  system [22]. During transition from structure to another, positional symmetry of  $(\text{BO}_3)^{3-}$  and the number of types of boron atom positions in the lattice cell change.

## 6. Spectral characteristics of borates $\text{La}_{0.99-x}\text{Sc}_x\text{Eu}_{0.01}\text{BO}_3$

### 6.1. Luminescence spectra and luminescence excitation spectra of $\text{La}_{0.99}\text{Eu}_{0.01}\text{BO}_3$ , $\text{La}_{0.99}\text{Sc}_3\text{Eu}_{0.01}(\text{BO}_3)_4$ and $\text{Sc}_{0.99}\text{Eu}_{0.01}\text{BO}_3$

According to the X-ray diffraction analysis (Section 3), with an increase in Sc concentration,  $\text{La}_{0.99-x}\text{Sc}_x\text{Eu}_{0.01}\text{BO}_3$  initially have (A)  $\text{La}_{0.99}\text{Eu}_{0.01}\text{BO}_3$  aragonite structure, then, besides the aragonite,  $\text{La}_{0.99}\text{Sc}_3\text{Eu}_{0.01}(\text{BO}_3)_4$  (LSBO) lanthanum–scandium borate occurs and has huntite structure (*H*), and with  $x = 0.99$ ,  $\text{Sc}_{0.99}\text{Eu}_{0.01}\text{BO}_3$  orthoborate has calcite structure (*C*). luminescence spectra (LS) of these compounds are shown in Figures 7 and 8. In LS of  $\text{La}_{0.99}\text{Eu}_{0.01}\text{BO}_3$  with the aragonite structure, bands with  $\lambda_{\text{max}}$  are observed: 578.6 nm (2.143 eV) (electronic transition  ${}^5D_0 \rightarrow {}^7F_0$ ); 589.4, 591, 592.6 nm (2.103, 2.078, 2.092 eV) ( ${}^5D_0 \rightarrow {}^7F_1$ ); 611.6, 614.5, 617.4, 619.8, 623 nm (2.027, 2.018, 2.008, 2.0006, 1.990 eV) ( ${}^5D_0 \rightarrow {}^7F_2$ );  $\sim 653.5$  nm (1.897 eV) ( ${}^5D_0 \rightarrow {}^7F_3$ ); 681.6, 684, 700.6, 701.6 nm (1.819, 1.813, 1.77, 1.767 eV) ( ${}^5D_0 \rightarrow {}^7F_4$ ). Bands with  $\lambda_{\text{max}} = 614.5$  and 701.6 nm have the maximum intensity (Figure 7, spectrum 1; Figure 8, spectrum 1). Similar spectra were observed in [22–25].

LS of  $\text{La}_{0.99}\text{Sc}_3\text{Eu}_{0.01}(\text{BO}_3)_4$  contains bands with  $\lambda_{\text{max}} = 589.8, 595.7$  nm (2.102, 2.08 eV) ( $D_0 \rightarrow {}^7F_1$ ); 610.2,

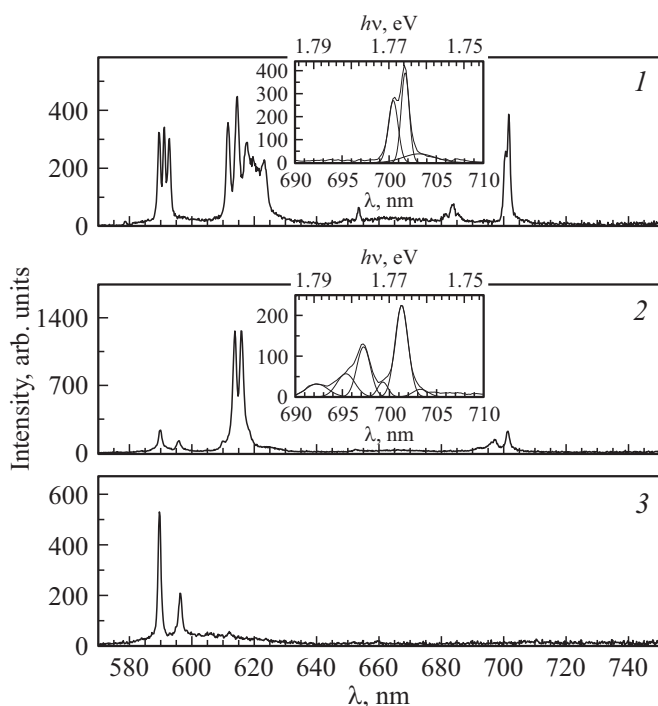


**Figure 7.** Luminescence spectra of borates 1 —  $\text{La}_{0.99}\text{Eu}_{0.01}\text{BO}_3$ ; 2 —  $\text{La}_{0.14}\text{Sc}_{0.85}\text{Eu}_{0.01}\text{BO}_3$ ; 3 —  $\text{Sc}_{0.99}\text{Eu}_{0.01}\text{BO}_3$ .  $\lambda_{\text{ex}} = 394$  nm. Insert shows 690–710 nm spectrum region decomposition. A linear energy scale was used for spectrum decomposition, and then transition from eV to nm was carried out.

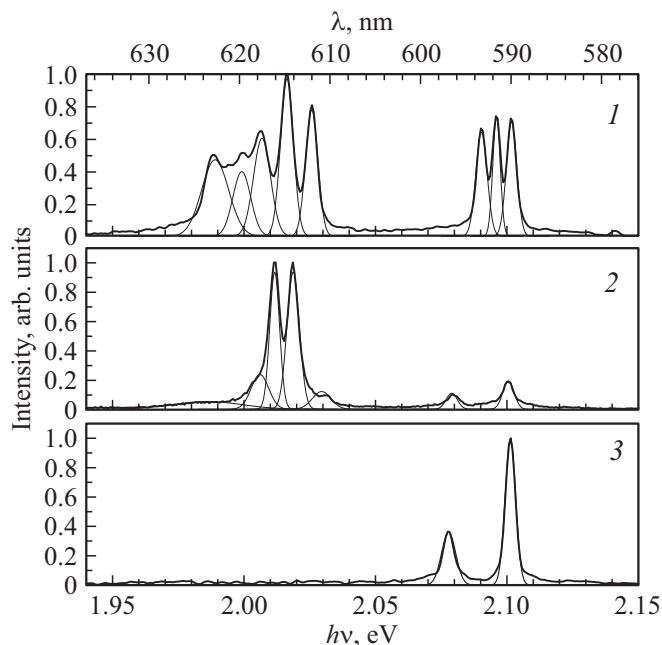


**Figure 8.** 580–630 nm (2.138–1.968 eV) spectrum region decomposition (Figure 7).

613.8, 615.8 nm (2.03, 2.02, 2.0136 eV) ( $^5D_0 \rightarrow ^7F_2$ ); 692.2, 697.4, 701.2 nm (1.709, 1.778, 1.768 eV) ( $^5D_0 \rightarrow ^7F_4$ ). Bands with  $\lambda_{\text{max}} = 613.8$  and 615.8 nm have the highest intensity (Figure 7, spectrum 2; Figure 8,

spectrum 2). Note that the luminescence spectrum of  $\text{EuAl}_3(\text{BO}_3)_4$  europium alumoborate with huntite structure studied in [59,60] contains bands 591, 596 nm ( $^5D_0 \rightarrow ^7F_1$ ); 613, 618 nm ( $^5D_0 \rightarrow ^7F_2$ );  $\sim 650$  nm ( $^5D_0 \rightarrow ^7F_3$ ); 699, 704 nm ( $^5D_0 \rightarrow ^7F_4$ ). Bands with  $\lambda_{\text{max}} = 613$  and 618 nm have the highest intensity. Luminescence spectrum of  $\text{La}_{0.99}\text{Sc}_3\text{Eu}_{0.01}(\text{BO}_3)_4$  is similar to LS of  $\text{EuAl}_3(\text{BO}_3)_4$ . Clear difference in position is observed between long-wavelength band of transition ( $^5D_0 \rightarrow ^7F_1$ ) and bands corresponding to transition ( $^5D_0 \rightarrow ^7F_4$ ).

In the luminescence spectrum of  $\text{Sc}_{0.99}\text{Eu}_{0.01}\text{BO}_3$  sample, bands with  $\lambda_{\text{max}} = 589.6$  and 596.2 nm (2.103 and 2.079 eV) ( $^5D_0 \rightarrow ^7F_1$ ) have the highest intensity. Their position is close to the position of bands in  $\text{LuBO}_3(\text{Eu})$  calcite modification [10–12] and in lanthanum-scandium borate corresponding to transition  $^5D_0 \rightarrow ^7F_1$  (589.8 and 595.7 nm). At the same time, the luminescence spectrum of  $\text{La}_{0.99-x}\text{Sc}_x\text{Eu}_{0.01}\text{BO}_3$  aragonite ( $0 \leq x < 0.37$ ) (Figure 7 and 8) is close to LS of  $\text{Eu}^{3+}$  in vaterite modification  $\text{ReBO}_3(\text{Eu})$ , where  $\text{Re} = (\text{Lu}, \text{Tb}, \text{Y}, \text{Gd})$ , containing bands in 588–596 nm ( $^5D_0 \rightarrow ^7F_1$ ), 608–613 and 624–632 nm ( $^5D_0 \rightarrow ^7F_2$ ) regions, with each of them consisting of several narrow bands [3,8–12].

Luminescence excitation spectra (LES) of the most intense luminescence bands of  $\text{La}_{0.99}\text{Eu}_{0.01}\text{BO}_3$ ,  $\text{La}_{0.99}\text{Sc}_3\text{Eu}_{0.01}(\text{BO}_3)_4$  and  $\text{Sc}_{0.99}\text{Eu}_{0.01}\text{BO}_3$  having aragonite, huntite and calcite structure, respectively, are shown in Figure 9, spectra 1, 3, 9. In LES of  $\text{La}_{0.99}\text{Eu}_{0.01}\text{BO}_3$  (LBO) and  $\text{La}_{0.99}\text{Sc}_3\text{Eu}_{0.01}(\text{BO}_3)_4$  (LSBO) wide band ( $\lambda = 230$ –330 nm) (charge transfer band — CTB) with maximums at  $\sim 280$  and  $\sim 278$  nm, respectively, is observed in UV spectrum. LES's of these samples also contain several narrow bands in the range of 290–500 nm corresponding to resonance excitation of  $\text{Eu}^{3+}$ . In the longwave region for LBO and LSBO, bands with maximums at  $\lambda_{\text{ex}} = 394$  and 395 nm ( $^7F_0 \rightarrow ^5L_6$ ) and 465.5 and 466 nm ( $^7F_0 \rightarrow ^5D_2$ ), respectively, are the most intense. Thus, LES of  $\text{La}_{0.99}\text{Eu}_{0.01}\text{BO}_3$  and  $\text{La}_{0.99}\text{Sc}_3\text{Eu}_{0.01}(\text{BO}_3)_4$  are close to each other.

The luminescence excitation spectrum of the most intense luminescence band of  $\text{Sc}_{0.99}\text{Eu}_{0.01}\text{BO}_3$  ( $\lambda_{\text{max}} = 589.6$  nm) having calcite structure (C) (Table) is shown in Figure 9, spectrum 9. It contains wide band 210–270 nm (CTB) with a maximum at  $\lambda_{\text{ex}} \sim 242$  nm and several bands in range 290–500 nm. Band  $\lambda_{\text{ex}} = 394$  nm corresponding to the resonant excitation of  $\text{Eu}^{3+}$  is the most intense. CTB intensity in these samples is  $\sim 15$  times as high as the intensity of band 394 nm. LES of  $\text{Sc}_{0.99}\text{Eu}_{0.01}\text{BO}_3$  is closer to LES of calcite modification of  $\text{LuBO}_3(\text{Eu})$  where CTB with a maximum at  $\sim \lambda_{\text{ex}} = 254$  nm is observed, and the CTB intensity is  $\sim 25$  times as high as the intensity of band 394 nm [10–12].

Rare-earth ions —  $\text{Re}^{3+}$  (including also  $\text{Eu}^{3+}$ ) are known to be sensitive to the nearest environment [61,62]. Therefore, the change in the local environment of  $\text{Re}^{3+}$  ions can be evaluated by the change in their spectral characteristics.  $\text{Eu}^{3+}$  ions allow to monitor the structural state both inside

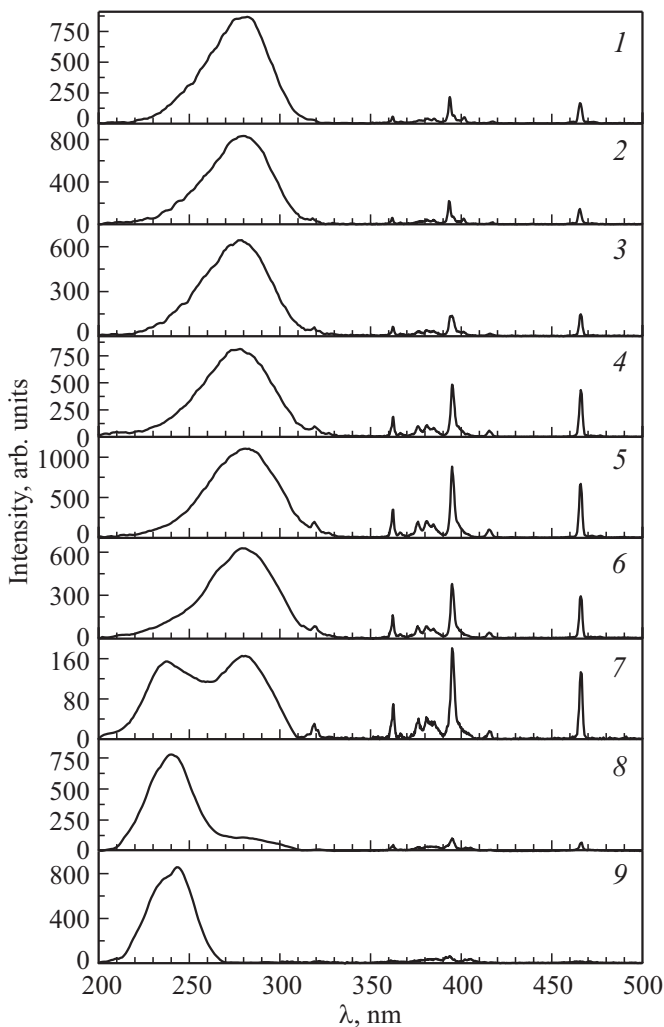


**Figure 9.** Luminescence excitation spectra of borates  $\text{La}_{0.99-x}\text{Sc}_x\text{Eu}_{0.01}\text{BO}_3$ . 1 —  $\text{La}_{0.99}\text{Eu}_{0.01}\text{BO}_3$ ; 2 —  $\text{La}_{0.73}\text{Sc}_{0.26}\text{Eu}_{0.01}\text{BO}_3$ ; 3 —  $\text{La}_{0.51}\text{Sc}_{0.48}\text{Eu}_{0.01}\text{BO}_3$ ; 4 —  $\text{La}_{0.24}\text{Sc}_{0.75}\text{Eu}_{0.01}\text{BO}_3$ ; 5 —  $\text{La}_{0.09}\text{Sc}_{0.9}\text{Eu}_{0.01}\text{BO}_3$ ; 6 —  $\text{La}_{0.09}\text{Sc}_{0.9}\text{Eu}_{0.01}\text{BO}_3$ ; 7 —  $\text{La}_{0.09}\text{Sc}_{0.9}\text{Eu}_{0.01}\text{BO}_3$ ; 8 —  $\text{La}_{0.02}\text{Sc}_{0.97}\text{Eu}_{0.01}\text{BO}_3$ ; 9 —  $\text{Sc}_{0.99}\text{Eu}_{0.01}\text{BO}_3$ . 1–3 —  $\lambda_{\text{max}} = 614.5 \text{ nm}$ ; 4–6 —  $\lambda_{\text{max}} = 613.8 \text{ nm}$ ; 7–9 —  $\lambda_{\text{max}} = 589.6 \text{ nm}$ .

and on surface of a sample. The information about the immediate environment of  $\text{Eu}^{3+}$  inside the sample may be obtained by exciting luminescence of  $\text{Eu}^{3+}$  using light with the energy corresponding to the resonance excitation of  $\text{Eu}^{3+}$  ( $\lambda_{\text{ex}} \sim 394$  and  $\sim 466 \text{ nm}$ ) in the transmission region of the samples ( $\lambda > 300 \text{ nm}$ ) [13–15]. Luminescence excitation of  $\text{Eu}^{3+}$  rare-earth ions by light with an energy within the intense absorption region of the sample ( $\lambda = 225\text{--}300 \text{ nm}$ ) — charge transfer band ( $\text{O}^{2-} (2p) \rightarrow \text{Eu}^{3+} (4f^6)$ ) [63] allows to obtain the information on local environment of  $\text{Eu}^{3+}$  ions in the near-surface crystal layer [13–15]. As shown in [64–66], when the short-range order surrounding  $\text{Eu}^{3+}$  ions is the same for the whole sample, which is supported by the coincidence of luminescence spectra (LS) of the

near-surface layer and sample volume, the sample is single-phase.

## 6.2. Luminescence excitation spectra of borates $\text{La}_{0.99-x}\text{Sc}_x\text{Eu}_{0.01}(\text{BO}_3)_4$

Luminescence excitation spectra (LES) of the most intense luminescence bands of  $\text{La}_{0.99-x}\text{Sc}_x\text{Eu}_{0.01}(\text{BO}_3)_4$  borates at  $x = 0.26, 0.48, 0.75, 0.9, 0.97$  and  $0.99$  are shown in Figure 9. LES of  $\text{La}_{0.73}\text{Sc}_{0.26}\text{Eu}_{0.01}\text{BO}_3$  ( $\lambda_{\text{max}} = 614.5 \text{ nm}$ ) having the aragonite structure (A) (Table) is almost the same as LES of  $\text{La}_{0.99}\text{Eu}_{0.01}\text{BO}_3$  (Figure 9, spectra 1, 2). It contains CTB with a maximum at  $\sim 280 \text{ nm}$  and several narrow resonant bands of  $\text{Eu}^{3+}$  ions with bands whose maximums are at  $\lambda_{\text{ex}} = 394$  and  $465.5 \text{ nm}$  being the most intense of them. Such luminescence excitation spectra with  $\lambda_{\text{max}} = 614.5 \text{ nm}$  are observed for samples containing 31, 37 and 48 at.%  $\text{Sc}^{3+}$ , which contain 82% (A), 18% huntite (H) (82A/18H); 73A/27H and 54A/46H, respectively (Figure 9, spectra 2, 3, Table). It should be noted that the intensity of the band with  $\lambda_{\text{ex}} = 394 \text{ nm}$  in these samples is  $\sim 4.5$  times lower than that of CTB. LES of the most intense luminescence band of  $\text{Eu}^{3+}$  ions ( $\lambda_{\text{max}} = 613.8 \text{ nm}$ ) in  $\text{La}_{0.99-x}\text{Sc}_x\text{Eu}_{0.01}(\text{BO}_3)_4$  at  $x = 0.6; 0.7; 0.75; 0.85$ , which have the following structures — 22A/78H; 7A/93H and 100H, respectively, contain a wide band (CTB) with a maximum at  $\lambda_{\text{ex}} = 278 \text{ nm}$  and bands with maximums at  $\lambda_{\text{ex}} = 395$  and  $466 \text{ nm}$  (Figure 9, spectra 4, 5). In LES of the band with  $\lambda_{\text{max}} = 613.8 \text{ nm}$ , corresponding to a trigonal modification of lanthanum-scandium borate, in  $\text{La}_{0.99-x}\text{Sc}_x\text{Eu}_{0.01}(\text{BO}_3)_4$  samples containing 90; 95 and 97 at.%  $\text{Sc}^{3+}$  having structures 64H/36C (C-calcite); 26H/74C and 13H/87C, respectively, CTB ( $\lambda_{\text{ex}} = 280 \text{ nm}$ ) and bands with  $\lambda_{\text{ex}} = 395$  and  $466 \text{ nm}$  are observed (Figure 9, spectra 6, 7). At the same time, in the luminescence excitation spectrum with  $\lambda_{\text{max}} = 589.6 \text{ nm}$  specific to the calcite modification of  $\text{Sc}_{0.99}\text{Eu}_{0.01}\text{BO}_3$  (Figure 8, spectrum 3), in  $\text{La}_{0.99-x}\text{Sc}_x\text{Eu}_{0.01}(\text{BO}_3)_4$  samples containing 90, 95 and 97 at.%  $\text{Sc}^{3+}$ , two CTBs ( $\lambda_{\text{ex}} \sim 240$  and  $280 \text{ nm}$ ) are observed in the UV region. In  $\text{La}_{0.09}\text{Sc}_{0.9}\text{Eu}_{0.01}\text{BO}_3$ , bands with  $\lambda_{\text{ex}} \sim 240$  and  $280 \text{ nm}$  have the same intensity, in  $\text{La}_{0.04}\text{Sc}_{0.95}\text{Eu}_{0.01}\text{BO}_3$  samples, intensity of  $240 \text{ nm}$  band is  $\sim 4.5$  times as high as that of  $280 \text{ nm}$  band. In borates containing 97 at.%  $\text{Sc}^{3+}$ , a band with  $\lambda_{\text{ex}} \sim 280 \text{ nm}$  occurs in the form of an shoulder on the longwave decline of  $240 \text{ nm}$  band (Figure 9, spectra 7, 8). LES of these samples also contain bands with  $\lambda_{\text{ex}} = 395$  and  $466 \text{ nm}$ . As reported above, the charge transfer band in LES for the most intense luminescence band of calcite modification  $\text{Sc}_{0.99}\text{Eu}_{0.01}\text{BO}_3$  ( $\lambda_{\text{max}} = 589.6 \text{ nm}$ ) has its maximum at  $\sim 240 \text{ nm}$  (Figure 9, spectrum 9). It should be noted that in luminescence excitation spectra with  $\lambda_{\text{max}} = 613.8 \text{ nm}$  of  $\text{La}_{0.99-x}\text{Sc}_x\text{Eu}_{0.01}(\text{BO}_3)_4$  samples containing 60–97 at.%  $\text{Sc}^{3+}$ , intensity of resonance band ( $395 \text{ nm}$ ) ( $I_{\text{Eu}}$ ) with an increase in  $\text{Sc}^{3+}$  concentration initially grows with respect to the CTB intensity ( $I_{\text{CTB}}$ ), achieves its crest at 90 at.%  $\text{Sc}^{3+}$ , and then decreases.

$I_{Eu}/I_{CTB}$  at 60, 90 and 97 at.%  $Sc^{3+}$  is equal to 0.45, 0.8 and 0.6, respectively.

### 6.3. Luminescence spectra of borates

#### $La_{0.99-x}Sc_xEu_{0.01}(BO_3)_4$

Luminescence spectra (LS) of  $La_{0.99-x}Sc_xEu_{0.01}(BO_3)_4$  at  $x = 0, 0.26, 0.31, 0.48, 0.6, 0.7, 0.75, 0.9, 0.97$  and  $0.99$  in 580–635 nm spectral range with resonance excitation of  $Eu^{3+}$  and in the charge transfer band crest are shown in Figure 10. LS of near-surface layer ( $\lambda_{ex} = 280$  nm) and volume ( $\lambda_{ex} = 394$  nm) of  $La_{0.99}Eu_{0.01}BO_3$  which, according to X-ray diffraction analysis, has an aragonite structure (Table) coincide (Fig. 10, spectra 1 and 2). They contain, as reported, a 587.6 nm ( $^5D_0 \rightarrow ^7F_0$ ) band, 3 bands in range 587–595 nm ( $^5D_0 \rightarrow ^7F_1$ ), and 5 bands in range 610–630 nm ( $^5D_0 \rightarrow ^7F_2$ ). Luminescence spectra of  $La_{0.99-x}Sc_xEu_{0.01}BO_3$  at  $0 \leq x \leq 0.26$  having aragonite structure (A) (Table) according to the X-ray diffraction analysis are identical. In these samples, LS of the near-surface layer and volume of the sample coincide like in  $La_{0.99}Eu_{0.01}BO_3$  sample. In  $La_{0.68}Sc_{0.31}Eu_{0.01}BO_3$  samples containing 82A/18H (Table), the luminescence spectrum of the near-surface layer ( $\lambda_{ex} = 280$  nm) contain the bands specific to aragonite structure  $LaBO_3(Eu)$  (Figure 10, spectrum 3). In LS of this sample volume ( $\lambda_{ex} = 394$  nm), bands in range 587–595 nm corresponding to magnetic dipole transition (MDT)  $^5D_0 \rightarrow ^7F_1$  remain unchanged. At the same time, band intensity ratio in range 610–630 nm corresponding to electric dipole transition (EDT) ( $^5D_0 \rightarrow ^7F_2$ ) changes considerably (Figure 10, spectrum 4). EDT is known to be more sensitive to the variation of local environment around  $Re^{3+}$ , including also  $Eu^{3+}$  ions, than MDT [9,61,62]. Even larger changes are observed in LS of  $La_{0.62}Sc_{0.37}Eu_{0.01}BO_3$  and  $La_{0.51}Sc_{0.48}Eu_{0.01}BO_3$  sample volumes containing 73A/27H and 54A/46H, respectively, (Table) (Figure 10, spectrum 6). In LS of the near-surface layer of  $La_{0.51}Sc_{0.48}Eu_{0.01}BO_3$ , band intensity ratio changes in range 610–630 nm ( $^5D_0 \rightarrow ^7F_2$ ) (Figure 10, spectrum 5). In the luminescence spectrum of  $La_{0.39}Sc_{0.6}Eu_{0.01}BO_3$  (22A/78H) sample volume, bands with  $\lambda_{max} = 589.8, 595.7, 613.8, 615.8$  nm are observed (Figure 10, spectrum 8) which are specific to  $La_{0.99}Sc_3Eu_{0.01}(BO_3)_4$  (LSBO) (Figure 7, spectrum 2). Bands with  $\lambda_{max} = 591$  and 592.6 nm ( $^5D_0 \rightarrow ^7F_1$ ) (Figure 10, spectrum 8) present in LS prove that the volume of this sample still contains the aragonite phase. LS of the near-surface layer of  $La_{0.39}Sc_{0.6}Eu_{0.01}BO_3$  contains bands specific to aragonite — 587.6 nm, 3 bands in range 587–595 nm, as well as bands specific to lanthanum-scandium borate — 613.8, 615.8 nm, which have the highest intensity (Figure 10, spectrum 7). In the luminescence spectrum of  $La_{0.29}Sc_{0.7}Eu_{0.01}BO_3$  (7A/93H) sample volume, only bands specific to LSBO are observed. At the same time, LS of the near-surface layer, in addition to the bands specific to lanthanum-scandium borate, contains weak 591 and 592.6 nm bands

corresponding to aragonite structure  $LaBO_3(Eu)$  (Figure 10, spectra 9, 10). luminescence spectra of the volume and near-surface layer of  $La_{0.24}Sc_{0.75}Eu_{0.01}BO_3$  and  $La_{0.14}Sc_{0.85}Eu_{0.01}BO_3$  (100H, Table) coincide. They contain only the bands specific to trigonal structure (Figure 10, spectra 11, 12). The same spectra of sample excitation by light with  $\lambda_{ex}$  282 and 394 nm are observed for  $La_{0.08}Sc_{0.9}Eu_{0.01}BO_3$  (64H/36C),  $La_{0.04}Sc_{0.95}Eu_{0.01}BO_3$  (26H/74C) and  $La_{0.02}Sc_{0.97}Eu_{0.01}BO_3$  (13H/87C) samples (Figure 10, spectra 13–16). It should be noted that the luminescence of samples containing 90 and 95 at.%  $Sc^{3+}$  is  $\sim 2$  times as intense as that of samples containing 75, 85 and 97 at.%  $Sc^{3+}$ . Luminescence spectra of the near-surface layer ( $\lambda_{ex} = 242$  nm) and of volume ( $\lambda_{ex} = 394$  nm) of  $Sc_{0.99}Eu_{0.01}BO_3$  samples have the calcite structure (Table) coincide and contain bands with  $\lambda_{max} = 589.6$  and 596.2 nm (Figure 10, spectra 17, 18).

It should be noted that in the luminescence spectra of  $La_{0.99-x}Sc_xEu_{0.01}BO_3$  samples at  $x = 0.9, 0.95$  and  $0.97$ , which contain 36, 74 and 87% of calcite and 64, 26 and 13% of huntite, respectively (Figure 10, spectra 13–16), there is no clear evidence that these compounds contain a calcite phase. This is due to the following causes. As reported above, in LS of  $La_{0.99}Sc_3Eu_{0.01}(BO_3)_4$  (LSBO), 4 bands with  $\lambda_{max} = 589.8, 595.7, 613.8$  and 615.8 nm have the highest intensity. LS of  $Sc_{0.99}Eu_{0.01}BO_3$  (SBO) samples contain bands with  $\lambda_{max} = 589.6$  and 596.2 nm whose position is close to that of two first bands in LS of lanthanum-scandium borate. Moreover, resonance excitation bands of  $Eu^{3+}$  in LSBO ( $\lambda_{ex} = 395, 466$  nm) and SBO (394, 465.5 nm) almost coincide. Therefore, when any of these bands is excited in a sample containing huntite and calcite phases, luminescence of all four bands is observed (Figure 10, spectra 14, 16), and it does not seem possible to assess the contribution made by SBO calcite phase in this luminescence. At the same time, positions of UV band crest (CTB) in the luminescence excitation spectra of the most intense luminescence bands of LSBO ( $\lambda_{ex} = 280$  nm) and SBO ( $\lambda_{ex} = 240$  nm) differ considerably. This allows to observe luminescence primarily specific to SBO calcite when  $La_{0.99-x}Sc_xEu_{0.01}BO_3$  ( $0.9 \leq x \leq 0.99$ ) samples are excited by light with  $\lambda_{ex} = 240$  nm or with  $\lambda_{ex} = 280$  nm for LSBO huntite. Figure 10 shows borate luminescence spectra 13, 15 at  $\lambda_{ex} = 280$  nm, because the luminescence excitation spectrum of most intense luminescence bands of these samples ( $\lambda_{max} = 613.8$  and 615.8 nm) has its maximum at  $\lambda_{ex} = 280$  nm (Figure 10, spectra 5, 6).

Figure 11 shows luminescence spectra of  $La_{0.99-x}Sc_xEu_{0.01}BO_3$  samples containing 90, 95 and 97 at.%  $Sc^{3+}$ , when  $Sc_{0.99}Eu_{0.01}BO_3$  ( $\lambda_{ex} = 240$  nm) calcite modification is excited in CTB. In LS of  $La_{0.09}Sc_{0.9}Eu_{0.01}BO_3$  samples containing 90 at.%  $Sc^{3+}$  (64H/36C (Table)), besides the bands specific to the calcite phase (589.6 and 596.2 nm), bands with  $\lambda_{max} = 610.2, 613.8, 615.8$  nm of  $LaSc_3(BO_3)_4(Eu)$  huntite structure are observed (Figure 11, spectrum 1). In LS of borate containing 95 at.%  $Sc^{3+}$  (26H/74C), band intensity of SBO

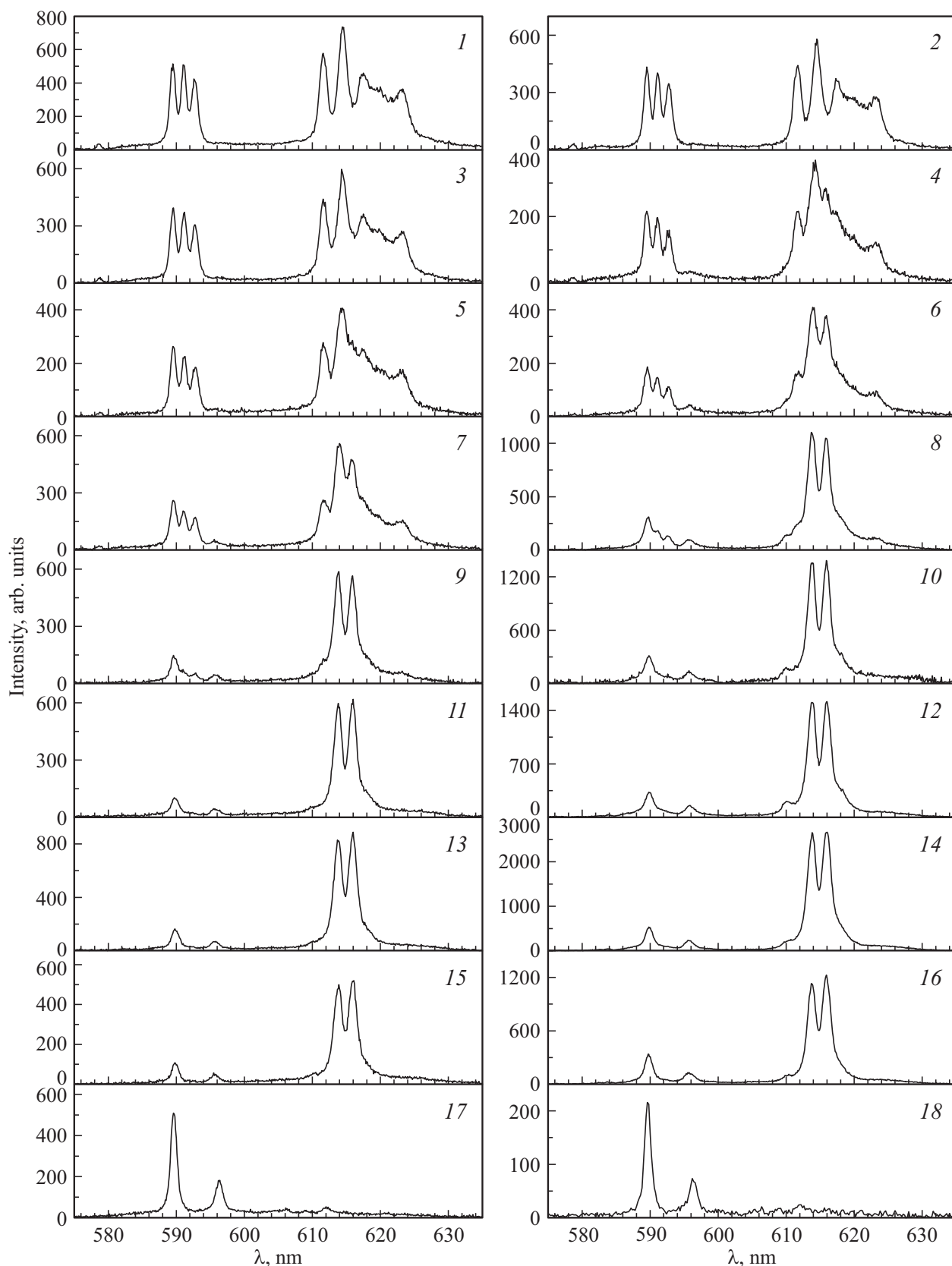


**Figure 10.** Luminescence spectra of borates  $\text{La}_{0.99-x}\text{Sc}_x\text{Eu}_{0.01}\text{BO}_3$ . 1, 2 —  $\text{La}_{0.99}\text{Eu}_{0.01}\text{BO}_3$ ; 3, 4 —  $\text{La}_{0.68}\text{Sc}_{0.31}\text{Eu}_{0.01}\text{BO}_3$ ; 5, 6 —  $\text{La}_{0.51}\text{Sc}_{0.48}\text{Eu}_{0.01}\text{BO}_3$ ; 7, 8 —  $\text{La}_{0.39}\text{Sc}_{0.6}\text{Eu}_{0.01}\text{BO}_3$ ; 9, 10 —  $\text{La}_{0.29}\text{Sc}_{0.7}\text{Eu}_{0.01}\text{BO}_3$ ; 11, 12 —  $\text{La}_{0.24}\text{Sc}_{0.75}\text{Eu}_{0.01}\text{BO}_3$ ; 13, 14 —  $\text{La}_{0.09}\text{Sc}_{0.9}\text{Eu}_{0.01}\text{BO}_3$ ; 15, 16 —  $\text{La}_{0.02}\text{Sc}_{0.97}\text{Eu}_{0.01}\text{BO}_3$ ; 17, 18 —  $\text{Sc}_{0.99}\text{Eu}_{0.01}\text{BO}_3$ . 1, 3, 5, 7, 9, 11, 13, 15 —  $\lambda_{\text{ex}} = 282$  nm; 17 —  $\lambda_{\text{ex}} = 244$  nm; 2, 4, 6, 8, 10, 12, 14, 16, 18 —  $\lambda_{\text{ex}} = 394$  nm.

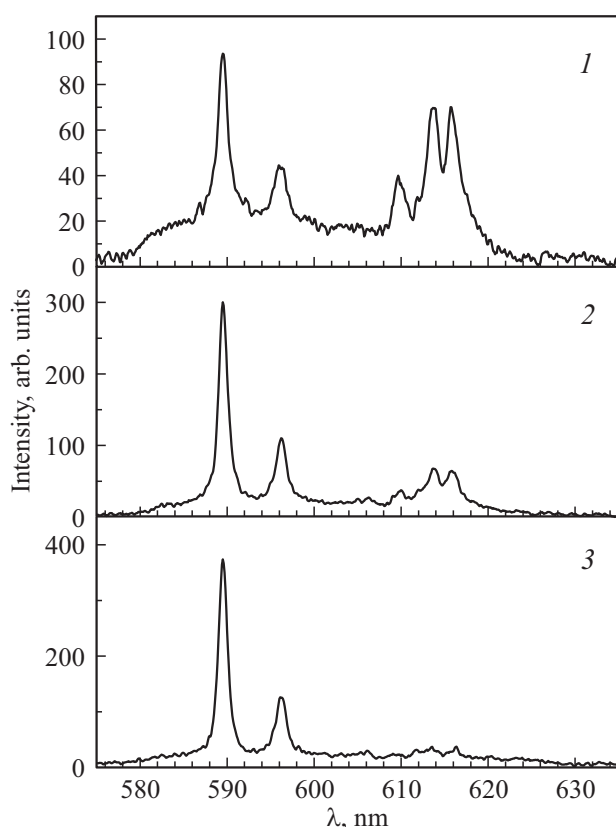


**Figure 11.** Luminescence spectra of borates. 1 —  $\text{La}_{0.09}\text{Sc}_{0.9}\text{Eu}_{0.01}\text{BO}_3$ ; 2 —  $\text{La}_{0.04}\text{Sc}_{0.95}\text{Eu}_{0.01}\text{BO}_3$ ; 3 —  $\text{La}_{0.02}\text{Sc}_{0.97}\text{Eu}_{0.01}\text{BO}_3$ .  $\lambda_{\text{ex}} = 240$  nm.

calcite modification grows and band intensity of LSBO trigonal modification decreases (Figure 11, spectrum 2). LS of  $\text{La}_{0.02}\text{Sc}_{0.97}\text{Eu}_{0.01}\text{BO}_3$  (13H/87C) samples (Figure 11, spectrum 3) coincides with LS of scandium orthoborate doped with  $\text{Eu}^{3+}$  (Figure 10, spectrum 17). Presence of  $\text{La}_{0.99-x}\text{Sc}_x\text{Eu}_{0.01}\text{BO}_3$  containing 90 and 95 at.%  $\text{Sc}^{3+}$  and bands specific to  $\text{LaSc}_3(\text{BO}_3)_4(\text{Eu})$  in LS, when luminescence is excited in  $\text{Sc}_{0.99}\text{Eu}_{0.01}\text{BO}_3$  ( $\lambda_{\text{ex}} = 240$  nm) CTB, is attributed to the fact that charge transfer bands in  $\text{LaSc}_3(\text{BO}_3)_4(\text{Eu})$  ( $\lambda_{\text{ex}} = 280$  nm) and  $\text{Sc}_{0.99}\text{Eu}_{0.01}\text{BO}_3$  ( $\lambda_{\text{ex}} = 240$  nm) are overlapping (Figure 9, spectra 4, 9). Therefore, when  $\text{La}_{0.99-x}\text{Sc}_x\text{Eu}_{0.01}\text{BO}_3$  samples are excited at  $0.9 \leq x \leq 0.97$  by light with  $\lambda_{\text{ex}} = 240$  nm, the luminescence spectrum of these samples, besides the bands specific to  $\text{Sc}_{0.99}\text{Eu}_{0.01}\text{BO}_3$  calcite modification, may contain bands specific to  $\text{LaSc}_3(\text{BO}_3)_4(\text{Eu})$  trigonal phase.

Therefore, comparison of the X-ray diffraction analysis data and spectroscopic measurements shows a correspondence between the structure and spectral characteristics of  $\text{La}_{0.99-x}\text{Sc}_x\text{Eu}_{0.01}\text{BO}_3$  at  $0 \leq x \leq 0.99$  orthoborates. Investigation of the luminescence spectra of the near-surface layer and volume of  $\text{La}_{0.99-x}\text{Sc}_x\text{Eu}_{0.01}(\text{BO}_3)_4$  orthoborates suggests that  $\text{La}_{0.99}\text{Sc}_3\text{Eu}_{0.01}(\text{BO}_3)_4$  lanthanum-scandium borate with trigonal huntite structure is formed at  $x \geq 0.31$  initially in the volume of the samples having the aragonite

structure. With a further increase in  $\text{Sc}^{3+}$  concentration, the trigonal phase is also formed on the sample surface. This process is similar to formation of vaterite phase in the volume of  $\text{La}_{0.98-x}\text{Lu}_x\text{Eu}_{0.02}\text{BO}_3$  microcrystals having the aragonite structure [22].

## 7. Conclusion

This study has investigated the structure, morphology, IR spectra, luminescence excitation spectra and luminescence spectra of the near-surface layer and volume of  $\text{La}_{0.99-x}\text{Lu}_x\text{Sc}_{0.01}\text{BO}_3$  borates synthesized at  $970^\circ\text{C}$  with  $0 \leq x \leq 0.99$ .

Well-defined correspondence between the structural modification and spectral photoluminescence characteristics and IR spectra of these compounds is established. The study of luminescence spectra at various excitation light wavelengths allowed to obtain information on the structure of near-surface layer and volume of the examined samples.

It is shown that in  $\text{La}_{0.99-x}\text{Sc}_x\text{Eu}_{0.01}\text{BO}_3$  borates with an increase in  $\text{Sc}^{3+}$  concentration, three compounds are gradually formed —  $\text{LaBO}_3$  lanthanum orthoborate,  $\text{LaSc}_3(\text{BO}_3)_4$  lanthanum-scandium borate,  $\text{ScBO}_3$  scandium orthoborate.

— With  $0 \leq x \leq 0.26$ , the samples are single-phase and have  $\text{LaBO}_3$  orthorhombic structure, space group  $Pnam$  (aragonite). The luminescence spectra of  $\text{Eu}^{3+}$  corresponding to the aragonite phase contain bands with  $\lambda_{\text{max}} = 578.6$  nm (transition  ${}^5D_0 \rightarrow {}^7F_0$ ); 589.4, 591 and 592.6 nm ( ${}^5D_0 \rightarrow {}^7F_1$ ); 611.6, 614.5, 617.4, 619.8, 621.3 and 623 nm ( ${}^5D_0 \rightarrow {}^7F_2$ );  $\sim 653.5$  nm ( ${}^5D_0 \rightarrow {}^7F_3$ ); 681.6, 684, 700.6, 701.6 nm ( ${}^5D_0 \rightarrow {}^7F_4$ ) in the near-surface layer and volume of microcrystals of these samples. The IR spectra contain absorption bands 593, 613, 723, 789, 940 and  $1306\text{ cm}^{-1}$ , which correspond to the aragonite phase.

— With  $0.26 < x < 0.75$ , the samples are two-phase — besides the aragonite structure,  $\text{LaSc}_3(\text{BO}_3)_4$  trigonal structure, space group  $R32H$  is observed. With increase in  $\text{Sc}^{3+}$  concentration, relative amount of huntite grows, while relative amount of aragonite decreases. In luminescence spectra and IR spectra, bands specific to  $\text{La}_{0.99}\text{Eu}_{0.01}\text{BO}_3$  aragonite structure and  $\text{La}_{0.99-x}\text{Sc}_3\text{Eu}_{0.01}(\text{BO}_3)_4$  huntite structure are observed.

— With  $0.75 \leq x \leq 0.85$ ,  $\text{LaSc}_3(\text{BO}_3)_4$  lanthanum-scandium borate is observed. Luminescence spectra of  $\text{Eu}^{3+}$  in these samples contain bands with  $\lambda_{\text{max}} = 589.8, 595.7$  nm ( ${}^5D_0 \rightarrow {}^7F_1$ ); 610.2, 613.8, 615.8 nm ( ${}^5D_0 \rightarrow {}^7F_2$ ); 692.2, 697.4, 701.2 nm ( ${}^5D_0 \rightarrow {}^7F_4$ ). Bands with  $\lambda_{\text{max}} = 613.8$  and 615.8 nm have the highest intensity. In IR spectra of huntite, absorption bands 665, 717, 752, 775, 968, 1234,  $1338\text{ cm}^{-1}$  are observed.

— With  $0.85 < x \leq 0.97$ , the samples are two-phase and contain  $\text{LaSc}_3(\text{BO}_3)_4$  huntite and  $\text{ScBO}_3$  calcite, space group  $R\bar{3}c$ . With increase in  $\text{Sc}^{3+}$  concentration, relative amount of calcite grows, while relative amount of huntite decreases. Luminescence spectra and IR spectra contain

the bands specific to huntite and calcite modifications of these samples.

– With  $0.97 < x \leq 0.99$ , the samples have  $\text{ScBO}_3$  calcite structure. In the luminescence spectrum of  $\text{Sc}_{0.99}\text{Eu}_{0.01}\text{BO}_3$  sample, bands with  $\lambda_{\text{max}} = 589.6$  and  $596.2 \text{ nm}$  ( ${}^5D_0 \rightarrow {}^7F_1$ ) have the highest intensity. In IR spectra, absorption bands  $644$ ,  $752$ ,  $775$ , and  $1279 \text{ cm}^{-1}$  are observed.

Thus, in  $\text{La}_{0.99-x}\text{Sc}_x\text{Eu}_{0.01}\text{BO}_3$  with an increase in  $\text{Sc}^{3+}$  concentration in the charge, gradual change of structural states is observed:  $\text{LaBO}_3$  aragonite ( $0 \leq x \leq 0.26$ )  $\rightarrow$  aragonite + huntite  $\text{LaSc}_3(\text{BO}_3)_4$  ( $0.26 < x < 0.75$ )  $\rightarrow$  huntite ( $0.75 \leq x \leq 0.85$ )  $\rightarrow$  huntite + calcite  $\text{ScBO}_3$  ( $0.85 < x \leq 0.97$ )  $\rightarrow$  calcite ( $0.97 < x \leq 0.99$ ).

It was found that, with an increase in  $x$ ,  $\text{La}_{0.99-x}\text{Sc}_x\text{Eu}_{0.01}(\text{BO}_3)_4$  huntite is initially formed in the volumes of  $\text{La}_{0.99-x}\text{Sc}_x\text{Eu}_{0.01}\text{BO}_3$  samples initially having the aragonite structure. The further increase in  $\text{Sc}^{3+}$  concentration results in the formation of huntite structure throughout the sample.

Morphology study of  $\text{La}_{0.99-x}\text{Sc}_x\text{Eu}_{0.01}\text{BO}_3$  ( $0 \leq x \leq 0.99$ ) borate microparticles suggests that  $\text{La}_{0.99}\text{Sc}_3\text{Eu}_{0.01}(\text{BO}_3)_4$  samples having a huntite structure contain elongated microcrystals  $0.3\text{--}1 \times 1\text{--}4 \mu\text{m}$  in size in the form of well faceted columns with pyramidal opposite ends.  $\text{La}_{0.99}\text{Eu}_{0.01}\text{BO}_3$  aragonite orthoborates and  $\text{Sc}_{0.99}\text{Eu}_{0.01}\text{BO}_3$  calcite orthoborates contain microcrystals  $1\text{--}6 \mu\text{m}$  and  $1\text{--}3 \mu\text{m}$  in size, respectively.

$\text{La}_{0.99-x}\text{Sc}_x\text{Eu}_{0.01}\text{BO}_3$  have high luminescence intensity and may be used as high-performance red phosphors for LED light sources.

## Acknowledgments

The authors thank the Research Facility Center of ISSP RAS for the morphology study of the samples and their characterization by IR spectroscopy and X-ray diffraction analysis methods.

## Funding

The research is carried out within the state task of ISSP RAS.

## Conflict of interest

The authors declare that they have no conflict of interest.

## References

- [1] E.F. Shubert, J.K. Kim. *Science* **308**, 1274 (2005).
- [2] X. Zhang, X. Fu, J. Song, M.-L. Gong. *Mater. Res. Bull.* **80**, 177 (2016).
- [3] C. Mansuy, J.M. Nedelec, C. Dujardin, R. Mahiou. *Opt. Mater.* **29**, 6, 697 (2007).
- [4] J.-P. Meyu, T. Jensen, G. Huber. *IEEE J. Quantum Electron* **30**:913 (1994).
- [5] D. Lu, Z. Pan, H. Zwang, J. Wang. *Opt. Mater. Express* **5**, 8, 1822 (2015).
- [6] A.B. Kuznetsov, K.A. Kokh, N.G. Kononova, V.S. Shevchenko, S.V. Rashchenko, D.M. Ezhov, A.Y. Jamous, A. Bolatov, B. Uralbekov, V.A. Svetlichnyi, A.E. Kokh. *J. Alloys Comp.* **851**, 156825 (2021).
- [7] V.V. Mikhailin, D.A. Spassky, V.N. Kolobanov, A.A. Meotishvili, D.G. Permenov, B.I. Zadneprovski. *Rad. Measurements* **45**, 307 (2010).
- [8] J. Yang, G. Zhang, L. Wang, Z. You, S. Huang, H. Lian, J. Lin. *J. Solid State Chem.* **181**, 2672 (2008).
- [9] G. Blasse, B.C. Grabmaier. *Luminescent Materials*. Springer-Verlag, Berlin–Heidelberg (1994). 233 p.
- [10] Jun Yang, Chunxia Li, Xiaoming Zhang, Zewei Quan, Cuimiao Zhang, Huaiyong Li, Jun Lin. *Chem. Eur. J.* **14**, 14, 4336 (2008).
- [11] S.Z. Shmurak, V.V. Kedrov, A.P. Kiselev, I.M. Shmyt'ko, *FTT* **57**, 1, 19 (2015). (in Russian).
- [12] S.Z. Shmurak, V.V. Kedrov, A.P. Kiselev, T.N. Fursova, I.M. Shmyt'ko. *FTT* **57**, 8, 1558 (2015). (in Russian).
- [13] S.Z. Shmurak, V.V. Kedrov, A.P. Kiselev, T.N. Fursova, I.I. Zver'kova, E.Yu. Postnova. *FTT* **63**, 7, 933 (2021). (in Russian).
- [14] S.Z. Shmurak, V.V. Kedrov, A.P. Kiselev, T.N. Fursova, I.I. Zver'kova, E.Yu. Postnova. *FTT* **63**, 10, 1615 (2021). (in Russian).
- [15] S.Z. Shmurak, V.V. Kedrov, A.P. Kiselev, T.N. Fursova, I.I. Zver'kova, *FTT* **62**, 12, 2110 (2020). (in Russian).
- [16] J. Hölsä. *Inorg. Chim. Acta* **139**, 1–2, 257 (1987).
- [17] E.M. Levin, R.S. Roth, J.B. Martin. *Am. Miner.* **46**, 9–10, 1030 (1961).
- [18] G. Chadeyron, M. El-Ghozzi, R. Mahiou, A. Arbus, C. Cousseins. *J. Solid State Chem.* **128**, 261 (1997).
- [19] D. Santamaría-Pérez, O. Gomis, J. Angel Sans, H.M. Ortiz, A. Vegas, D. Errandonea, J. Ruiz-Fuertes, D. Martínez-García, B. García-Domene, André L. J. Pereira, F. Javier Manjón, P. Rodríguez-Hernández, A. Muñoz, F. Piccinelli, M. Bettinelli, C. Popescu. *J. Phys. Chem. C* **118**, 4354 (2014).
- [20] Wen Ding, Pan Liang, Zhi-Hong Liu. *Mater. Res. Bull.* **94**, 31 (2017).
- [21] Wen Ding, Pan Liang, Zhi-Hong Liu. *Solid State Sci.* **67**, 76 (2017).
- [22] S.Z. Shmurak, V.V. Kedrov, A.P. Kiselev, T.N. Fursova, I.I. Zver'kova, S.S. Khasanov, *FTT* **63**, 12, 2142 (2021). (in Russian).
- [23] N.I. Steblevskaya, M.I. Belobeletskaya, M.A. Medkov. *Zhurn. neorgan. khimii* **66**, 4, 440 (2021). (in Russian).
- [24] J. Guang, C. Zhang, C. Wang, L. Liu, C. Huang, S. Ding. *Cryst. Eng. Commun.* **14**, 579 (2012).
- [25] J. Zhang, M. Yang, H. Jin, X. Wang, X. Zhao, X. Liu, L. Peng. *Mater. Res. Bull.* **47**, 247 (2012).
- [26] S.Z. Shmurak, V.V. Kedrov, A.P. Kiselev, T.N. Fursova, I.I. Zver'kova, *FTT* **64**, 8, 955 (2022). (in Russian).
- [27] S.Z. Shmurak, V.V. Kedrov, A.P. Kiselev, T.N. Fursova, I.I. Zver'kova, *FTT* **64**, 12, 2000 (2022). (in Russian).
- [28] S.Z. Shmurak, V.V. Kedrov, A.P. Kiselev, T.N. Fursova, I.I. Zver'kova, *FTT* **64**, 4, 474 (2022). (in Russian).
- [29] S.Z. Shmurak, V.V. Kedrov, A.P. Kiselev, T.N. Fursova, I.I. Zver'kova, *FTT* **65**, 2, 312 (2023). (in Russian).
- [30] Heng-Wei Wei, Li-Ming Shao, Huan Jiao, Xi-Ping Jing. *Opt. Mater.* **75**, 442 (2018).

- [31] R. Nayar, S. Tamboli, A.K. Sahu, V. Nayar, S.J. Dhoble. *J. Fluoresc.* **27**, 251 (2017).
- [32] S.K. Omanwar, N.S. Savala *Appl. Phys. A* **123**, 673 (2017).
- [33] A. Haberer, Kaindl R, Huppertz H. *Z. Naturforsch. Chem. Sci. B* **65**, 1206 (2010).
- [34] R. Velchuri, B.V. Kumar, V.R. Devi, G. Prasad, D.J. Prakash, M. Vital. *Mater. Res. Bull.* **46**, 8, 1219 (2011).
- [35] Jin Teng-Teng, Zhang Zhi-Jun, Zhang Hui, Zhao Jing-Tai. *J. Inorganic Mater.* **28**, 10, 1153 (2013).
- [36] K.K. Palkina, V.G. Kuznetsov, L.A. Butman, B.F. Dzhurinsky, *Koordinatsionnaya khimiya* **2**, 2, 286 (1976). (in Russian).
- [37] S. Lemanceau, G. Bertrand-Chadeyron, R. Mahiou, M. El-Ghozzi, J.C. Couscins, P. Conflant, R.N. Vannier. *J. Solid State Chem.* **148**, 229 (1999).
- [38] N. Akçamlı, D. Ağaogulları, Ö. Balcı, M. Lütfi Oveçoğlu, İ. Duman. *Ceram. Int.* **42**, 10045 (2016).
- [39] C.E. Weir, E.R. Lippincott. *J. RES. Natl. Bur. Std.-A. Phys. Chem. A* **65**, 3, 173 (1961).
- [40] A. Szczeszak, T. Grzyb, St. Lis, R.J. Wiglusz. *Dalton Transact.* **41**, 5824 (2012).
- [41] Ling Li, Shihong Zhou, Siyuan Zhang. *Solid State Sci.* **10**, 1173 (2008).
- [42] D.A. Keszler, H. Sun, *Acta Crystallogr. Cryst. Struct. Commun. C* **44**, 1505 (1988).
- [43] I.M. Shmytko. *FTT* **61**, 11, 2210 (2019). (in Russian).
- [44] M. He, G. Wang, Z. Lin, W. Chen, S. Lu, Q. Wu. *Mater. Res. Innovation* **2**, 345 (1999).
- [45] G. Wang, M. He, W. Chen, Z. Lin, S. Lu, Q. Wu. *Mater. Res. Innovat.* **2**, 6, 341 (1999).
- [46] A.G. Ryabukhin, *Izv. Chelyabinskogo nauch. tsentra* **4**, 33 (2000). (in Russian).
- [47] C.E. Weir, E.R. Lippincott. *J. Res. Natl. Bur. Std.* **65A**, 3, 173 (1961).
- [48] W.C. Steele, J.C. Decius. *J. Chem. Phys.* **25**, 6, 1184 (1956).
- [49] A.D. Mills. *Inorganic Chem.* **1**, 4, 960 (1962).
- [50] I.A. Kaurova, D.M. Gorshkov, G.M. Kuz'micheva, V.B. Rybakov. *Fine Chem. Technol.* **13**, 6, (2018).
- [51] V.S. Kurazhkovskaya, E.Yu Borovikova, N.I. Leonyuk, E.V. Koporulina, E.L. Belokoneva. *Zhurn.struct. khimii* **49**, 6, 1074 (2008). (in Russian).
- [52] V.S. Kurazhkovskaya, E.A. Dobretsova, E.Yu Borovikova, V.V. Mal'tsev, N.I. Leonyuk. *Zhurn.struct. khimii* **52**, 4, 721 (2011). (in Russian).
- [53] E.Yu. Borovikova, E.A. Dobretsova, K.N. Boldyrev, V.S. Kurazhkovskaya, V.V. Maltsev, N.I. Leonyuk. *Vibrational Spectroscopy* **68**, 82 (2013).
- [54] E.A. Dobretsova, E.Yu Borovikova, K.N. Boldyrev, V.S. Kurazhkovskaya, N.I. Leonyuk. *Optika i spektroskopiya* **116**, 1, 85 (2014). (in Russian).
- [55] E.Yu. Borovikova, K.N. Boldyrev, S.M. Aksenov, E.A. Dobretsova, V.S. Kurazhkovskaya, N.I. Leonyuk, A.E. Savon, D.V. Deyneko. *Opt. Mater.* **49**, 304 (2015).
- [56] E. Belokoneva, A. Azizov, N. Leonyuk. *Zhurn. strukt. khimii* **22**, 3, 196 (1981). (in Russian).
- [57] N.I. Leonyuk, A.V. Pashkova, T.I. Timchenko. *Kristallografiya* **33**, 5, 1287 (1988). (in Russian).
- [58] E.L. Belokoneva, T.I. Timchenko. *Kristallografiya* **28**, 6, 1118 (1983). (in Russian).
- [59] G.E. Malashevich, V.N. Sigaev, N.V. Golubev, E.Kh. Mammadzhanova, A.V. Danilchik, A.V. Zubelevich, E.V. Lutsenko. *Pis'ma v ZhETF* **92**, 8, 547 (2010). (in Russian).
- [60] S.Z. Shmurak, V.V. Kedrov, A.P. Kiselev, I.I. Zver'kova. *FTT* **55**, 2, 336 (2013). (in Russian).
- [61] M.A. Elyashevich, *Spektroskopiya redkikh zemel'*, GITTL, M. (1953). 456 p. (in Russian).
- [62] M.I. Gaiduk, V.F. Zolin, L.S. Gaigerova. *Spektry lyuminestsii evropiya. Nauka, M.* (1974), 195 p. (in Russian).
- [63] A. Mayolet, W. Zhang, P. Martin, B. Chassigneux, J.C. Krupa. *J. Electrochem. Soc.* **143**, 1, 330 (1996).
- [64] S.Z. Shmurak, A.P. Kiselev, V.V. Sinitsyn, I.M. Shmytko, A.S. Aronin, B.S. Red'kin, E.G. Ponyatovsky, *FTT* **48**, 1, 48 (2006). (in Russian).
- [65] S.Z. Shmurak, A.P. Kiselev, N.V. Klassen, V.V. Sinitsyn, I.M. Shmytko, B.S. Red'kin, S.S. Khasanov. *IEEE Trans. Nucl. Sci.* **55**, 1-3, 1128 (2008).
- [66] S.Z. Shmurak, A.P. Kiselev, D.M. Kurmasheva, B.S. Red'kin, V.V. Sinitsyn, *ZhETF* **137**, 5, 867 (2010). (in Russian).

*Translated by E.Ilyinskaya*